Indonesian Journal on Geoscience Vol. 13 No. 2 August 2026: 243-267

INDONESIAN JOURNAL ON GEOSCIENCE
Geological Agency
Ministry of Energy and Mineral Resources

Journal homepage: https://ijog.geologi.esdm.go.id
ISSN 2355-9314, e-ISSN 2355-9306

Petrology, Geochemistry, and Peak Pressure-Temperature Metamorphism of Pinoh Metamorphic Rocks in The Schwaner Mountains, Indonesia

Nugroho Imam Setiawan[1], Agung Harijoko[1], Rahmadi Hidayat[1], I Gde Sukadana[2], Frederikus Dian Indrastomo[2], and Isyqi[3]

[1]Geological Engineering Department, Faculty of Engineering, Universitas Gadjah Mada, Yogyakarta, Indonesia
[2]Research Center for Nuclear Energy, National Research and Innovation Agency, Tangerang Selatan, Indonesia
[3]Research Center for Geological Resources, National Research and Innovation Agency, Bandung, Indonesia

Corresponding author: aharijoko@ugm.ac.id
Manuscript received: October, 25, 2024; revised: March, 11, 2025;
approved: May, 04, 2026; available online: July, 17, 2026

Abstract - The Pinoh Metamorphic Rocks in the Schwaner Mountains predominantly underwent contact metamorphism near a granitoid body, oriented E–W and NW–SE. The whole-rock geochemical analyses indicate that these metapelites are characterized by high Al_2O_3 (16.6–22.0 wt.%), moderate SiO_2 (60.0–67.7 wt.%), low CaO and Na_2O, and enrichment in large-ion lithophile elements relative to high field strength elements. Trace-element and REE patterns normalized to upper continental crust show LREE enrichment, negative Sr anomalies, and variable Zr contents, suggesting significant sedimentary recycling. Chemical weathering indices (CIA = 79–89; CIW = 89–99) and low ICV values (0.58–0.75) indicate compositionally mature pelitic to semipelitic protoliths. Provenance discrimination diagrams suggest derivation mainly from intermediate to felsic-igneous sources, with minor mafic contributions, deposited in an active continental margin to continental arc setting. Integrated petrographic, microstructural, mineral-chemical, thermobarometric, and phase equilibria analyses of samples from the Nanga Pinoh and Nanga Semalam areas reveal two main metamorphic events (M_1 and M_2). The M_1 event formed the primary S_1 foliation, whereas the M_2 event is marked by the growth of andalusite porphyroblasts and the occurrence of spotted biotite. Garnet locally nucleated during late M_1, but was chemically re-equilibrated during M_2. Peak metamorphic conditions of the garnet–andalusite–biotite schist, estimated using garnet–biotite–andalusite–quartz (GBAQ) geothermobarometry and pseudosection modeling, yield P–T conditions of 525–586° C at 2.0–3.8 kbar, consistent with low-pressure, high-temperature Buchan-type contact metamorphism related to Cretaceous granitoid magmatism in The Schwaner Mountains.

Keywords: geochemistry, peak pressure and temperature metamorphism, pseudosection, Pinoh Metamorphic Rocks, Schwaner Mountains

How to cite this article:
Setiawan, N.I., Harijoko, A., Hidayat, R., Sukadana, I.G., Indrastomo, F.D., and Isyqi, 2026. Petrology, Geochemistry, and Peak Pressure-Temperature Metamorphism of Pinoh Metamorphic Rocks in The Schwaner Mountains, Indonesia. *Indonesian Journal on Geoscience*, 13 (2), p.243-267. DOI:10.17014/ ijog.13.2.243-267

Introduction

Background

The Schwaner Mountains in southwestern Kalimantan are primarily composed of granitoids and metamorphic rocks, with minor volcanic and sedimentary rocks (Amiruddin and Trail, 1993). Hennig *et al.* (2017) divided the Schwaner Mountains are divided into three distinct zones: the Northwest Schwaner Zone

(NWSZ), the North Schwaner Zone (NSZ), and the South Schwaner Zone (SSZ), which exhibit rifting, subduction-related, and post-collisional magmatism, respectively. The NWSZ is part of the West Borneo Block and was positioned along the Sundaland margin during The Triassic. On the other hand, the NSZ and SSZ belong to the SW Borneo (Banda) Block, which separated from NW Australia during the Jurassic. Breitfeld *et al*. (2020) proposed that Jurassic within-plate or A-type granites in the SSZ were formed during the SW Borneo Block from NW Australia rifting, and were not associated with subduction. The Cretaceous igneous rocks in the NSZ and NWSZ represent magmatism from a volcanic arc related to subduction, occurring from approximately 135 Ma to 90-85 Ma. After subduction ceased around 90-85 Ma, at least two postcollisional magmatism phases were predominantly exposed in the SSZ.

The metamorphic rocks of the Pinoh Formation in the Schwaner Mountains were initially described by Bemmelen (1949), Haile (1974), and Amiruddin and Trail (1993). These rocks exhibit both regional and contact metamorphism. Previously, they were thought to be of Palaeozoic (Bemmelen, 1949; Haile, 1974; Tate, 1991) to Triassic ages (Pieters and Sanyoto, 1993), and were interpreted as representing an ancient continental basement (Bemmelen, 1949; Haile, 1974; Metcalfe, 1988). However, recent studies by Davies *et al*. (2014) and Breitfeld *et al*. (2020) have revised the age of the protolith (magmatic zircons) of these metamorphic rocks to the Early Cretaceous (c. 135-110 Ma), indicating that they were subsequently metamorphosed due to the emplacement of the Schwaner intrusions.

Breitfeld *et al*. (2020) carried out a detailed investigation of the Schwaner Mountains, which included an examination of the metamorphic rocks in the region. These metamorphic rocks are predominantly metapelites, with smaller quantities of metabasites and quartzites, mainly exposed in the NSZ. The metapelites consist primarily of andalusite-cordierite schists, andalusite schists, biotite schists, garnet-andalusite schists, garnet-sillimanite schists, and hornfels variants such as andalusite-cordierite hornfels. At least three major phases of deformation are documented: (1) low-grade metamorphism, (2) low-pressure, high-temperature metamorphism, and (3) shearing.

Geochemical analyses indicate that the protolith of the Pinoh metamorphic rocks had dacitic, rhyolitic, and basaltic compositions. Trace element spider diagrams suggest that the metamorphic rocks of the Pinoh Formation have geochemical affinities with the Menunuk Volcanics. This has led to the interpretation that the protolith of these metamorphic rocks was volcaniclastic sediment from the Menunuk Volcanics. This hypothesis is further supported by zircon geochronology, which shows that the oldest Cretaceous ages of the Pinoh metamorphic rocks are indistinguishable from those of the Menunuk Volcanics. Therefore, Breitfeld *et al*. (2020) concluded that the volcaniclastic sediments were deposited contemporaneously with the subduction-related volcanic rocks of the NSZ, and were later metamorphosed during the emplacement of Cretaceous granitoids.

Furthermore, zircon geochronology by Breitfeld *et al*. (2020) identified two major metamorphic events in the Pinoh metamorphic rocks. The first event, occurring around 120-110 Ma, is interpreted as thermal metamorphism caused by the intrusion of the Sepauk Tonalite. The second event, dated to approximately 90-80 Ma, is linked to thermal metamorphism associated with magmatic intrusions of The Asem Tonalite and The Sukadana Granite. Additionally, proposed that shearing in the Pinoh metamorphic rocks occurred during the Late Oligocene, based on fine-grained biotite ages ($^{40}Ar/^{39}Ar$) that are thought to be related to uplift and denudation in central Borneo.

The Menunuk volcanics exposed in the northern part of the Schwaner Mountains consist of felsic lithic tuff, volcaniclastic siltstone, mudstone, and turbiditic volcaniclastic rocks (Amiruddin and Trail, 1993). These volcanic rocks were interpreted as the downfaulted volcanic cover of the Sepauk Tonalite. Breitfeld *et al*. (2020) reported zircon U-Pb ages obtained by SHRIMP, indicating that these volcanic rocks date to 135-

125 Ma, making them the most likely protoliths of the Pinoh metamorphic rocks.

However, previous studies have not provided pressure-temperature (*P-T*) estimates for the metamorphic rocks of the Pinoh Formation. Evaluating the *P-T* conditions of these rocks is crucial for understanding the formation of their mineral associations, which may indicate either a single metamorphic event or a polymetamorphic evolution. Part of this evolution may be recorded in garnet, whose crystallochemical properties act as a 'black box', preserving aspects of earlier metamorphic processes (e.g., Serra-Varela *et al*., 2024). Thus, garnet composition is among the most commonly used proxies for *P-T* reconstructions in metapelite samples. Additionally, mineral phase equilibria modeling can predict chemical interactions among mineral assemblages and their mineral chemistry. Our recent fieldwork and new sampling of metamorphic rocks from the Schwaner Mountains, along with previous studies, form the basis for a new interpretation of the metamorphic development in this region. In this study, the Pinoh metamorphic rocks was re-evaluated by conducting a petrological analysis of garnet-bearing micaceous schists, combining mineral-chemistry studies, and estimating *P-T* conditions using conventional thermobarometry and phase equilibria analysis (pseudosection). This study aims to provide deeper insight into the protoliths and metamorphic history of these rocks. The hypothesis proposed here is that the Pinoh metamorphic rocks underwent polymetamorphism, including regional and contact metamorphic series, or that this occurred simultaneously with the intrusion of granitoids.

Geological Settings

The Schwaner Mountains comprise Jurassic-Cenozoic granitoids, including The Cretaceous Biwa Gabbro, Kerabai and Menunuk Volcanics, and Pinoh Metamorphic Rocks (Amiruddin and Trail, 1993; Haile *et al*., 1977; Williams *et al*., 1988). Sedimentary rocks, primarily located in the southwestern Schwaner Mountains, consist of Jurassic Ketapang siltstones, sandstones, shales, and tuffaceous rocks (Amiruddin and Trail, 1993). The granitoid belt spans approximately 200 km in width and at least 500 km in length, trending roughly east-west.

Hennig *et al*. (2017) subdivided the Schwaner Mountains into three zones: Northwest Schwaner Zone (NWSZ), North Schwaner Zone (NSZ), and South Schwaner Zone (SSZ), characterized by rifting, subduction-related, and postcollisional magmatism, respectively. The Sepauk Tonalite is the largest plutonic body within the Schwaner batholith, spanning the NWSZ and NSZ and potentially extending into parts of the SSZ (e.g., Hennig *et al*., 2017; Qian *et al*., 2022). This pluton predominantly comprises tonalite and granodiorite, with minor syenogranite, monzogranite, diorite, gabbro, and monzonite. It exhibits an I-type signature indicative of a subduction-related origin (*e.g.* Williams *et al*., 1988; Pieter and Sanyoto, 1993). Hennig *et al*. (2017) and Breitfeld *et al*. (2020) reported zircon ages of 101-81 Ma for the granitoids in the Laur and Sepauk plutons.

Hennig *et al*. (2017) suggest that the NWSZ belongs to early Mesozoic Sundaland and is distinguished by Triassic and Jurassic metagranitoids (Setiawan *et al*., 2013). Cretaceous igneous intrusions, such as the Sepauk Tonalite, Laur Granite, and Sukadana Granite, have intruded these older rocks (Pieter and Sanyoto, 1993; Breitfeld *et al*., 2020). The Laur Granite in the NWSZ is thought to be equivalent to the Sepauk Tonalite and Sukadana Granite found in the SSZ (Amiruddin and Trail, 1993; Pieter and Sanyoto, 1993). Similarly, in the NSZ, the Sepauk Tonalite is the largest igneous body in the NWSZ. The granitoids in the NWSZ were dated using the K-Ar method, yielding ages of approximately 128-107 Ma (Haile *et al*., 1977; Blandon *et al*., 1989). In the southern part of the NWSZ, granitoids with K-Ar ages of 87-77 Ma, potentially corresponding to the Sukadana Granite in the SSZ, were reported by Haile *et al*. (1977), Williams *et al*. (1988), and Blandon *et al*. (1989). U-Pb zircon ages provided by Hennig *et al*. (2017) support distinct magmatic phases at 118 ± 1.1 Ma, 101.5 ± 0.6 Ma, and 81.1 ± 1.1 Ma in the NWSZ. The Laur Granite and

Sepauk Tonalite were later intruded by the Late Cretaceous Biwa Gabbro in the NWSZ (Pieters and Sanyoto, 1993), with K-Ar dating giving an age of 88 ± 3.6 Ma (Blandon *et al*., 1989).

In the SSZ region, the Sukadana Granite, also referred to as the Ketapang Batholith, dates to approximately 85-79 Ma and predominantly consists of potassic granite and syenogranite, with U-Pb zircon ages indicating around 85-80 Ma (De Keyser and Rustandi, 1993; Hattum *et al*., 2013). The Sukadana Granite is interpreted as a post-collisional intrusion based on geochemical analysis (De Keyser and Rustandi, 1993). This granitoid was later intruded by the Sangiyang Granite at Bukit Sangiyang around 72 Ma (Breitfeld *et al*., 2020). Concurrent with the emplacement of the Sukadana Granite was the intrusion of smaller granitoid bodies near the Lupar Line in West Sarawak and Central Kalimantan.

Furthermore, Breitfeld *et al*. (2020) propose that the Northwest Sarawak Zone (NWSZ) was part of the West Borneo Block during the Triassic, located along the Sundaland margin. In contrast, the North and South Sarawak Zones (NSZ and SSZ) are components of the Southwest Borneo (Banda) Block, which separated from Northwest Australia during the Jurassic period. The Southwest Borneo Block collided with eastern Sundaland around 135 Ma. Subsequently, large I-type granitoid plutons and arc volcanics formed in the NWSZ and NSZ between approximately 90 and 132 Ma, in association with Cretaceous Paleo-Pacific subduction. The Jurassic granitoids in the SSZ are within-plate (A-type) granites believed to have formed during rifting. Postcollisional magmatism led to the formation of the Sukadana Granite, dated to 78-85 Ma, and the A-type Sangiyang Granite, dated to 72 Ma. There is no evidence for a continuous Triassic volcanic arc extending from Sundaland eastward across Borneo.

Volcanic rocks are widespread throughout the Schwaner Mountains and are primarily classified into the Menunuk and Kerabai Volcanics. The Menunuk Volcanics are composed of felsic lithic tuffs, volcaniclastic siltstones and mudstones, quartzites, and turbiditic volcaniclastic rocks and are primarily found in the northern region of The Schwaner Mountains (Amiruddin and Trail, 1993). Blandon *et al*. (1989) reported a whole-rock K-Ar age of 81.5 ± 2.8 Ma from an altered sample, interpreted as the age of metamorphism. In contrast, Breitfeld *et al*. (2020) reported zircon U-Pb ages determined by SHRIMP for the Menunuk Volcanics ranging from 135 to 125 Ma, suggesting that these may be the protoliths of the Pinoh metamorphic rocks. Wang *et al*. (2022) indicate that the Menunuk Volcanic is equivalent to the Raya Volcanic that formed at c. 144-130 Ma, which exhibits arc-like geochemical signatures. The Kerabai Volcanics are predominantly composed of mafic volcanic rocks and pyroclastics, with occasional rhyolites, and are exposed in the western and central region of the Schwaner Mountains (*e.g.* Amiruddin and Trail, 1993; Pieters and Sanyoto, 1993). These were interpreted as co-magmatic volcanic equivalents of the Sukadana Granite based on geochemical and stratigraphic evidence (De Keyser and Rustandi, 1993). Dykes associated with the Kerabai Volcanics were dated using K-Ar methods (the whole rock, hornblende, pyroxene), yielding Cretaceous ages of approximately 75-66 Ma (De Keyser and Rustandi, 1993; Pieters and Sanyoto, 1993).

The Pinoh Metamorphic Rocks are primarily located in the northern part of the Schwaner Mountains, predominantly within the NSZ area but extending into the NWSZ and SSZ (Figure 1). These metamorphic rocks consist mainly of interbedded, locally calcareous metapelites and fine quartz-rich metapsammites, with occasional intercalations of intermediate to mafic metavolcanic rocks. They have undergone regional metamorphism, intense deformation, and subsequent thermal metamorphism (Amiruddin and Trail, 1993; De Keyser and Rustandi, 1993; Pieters and Sanyoto, 1993). The progressive increase in metamorphic grade towards the intrusive tonalite bodies and the local occurrence of migmatites adjacent to these bodies indicate that the thermal metamorphism was associated with Early Cretaceous magmatism (Amiruddin

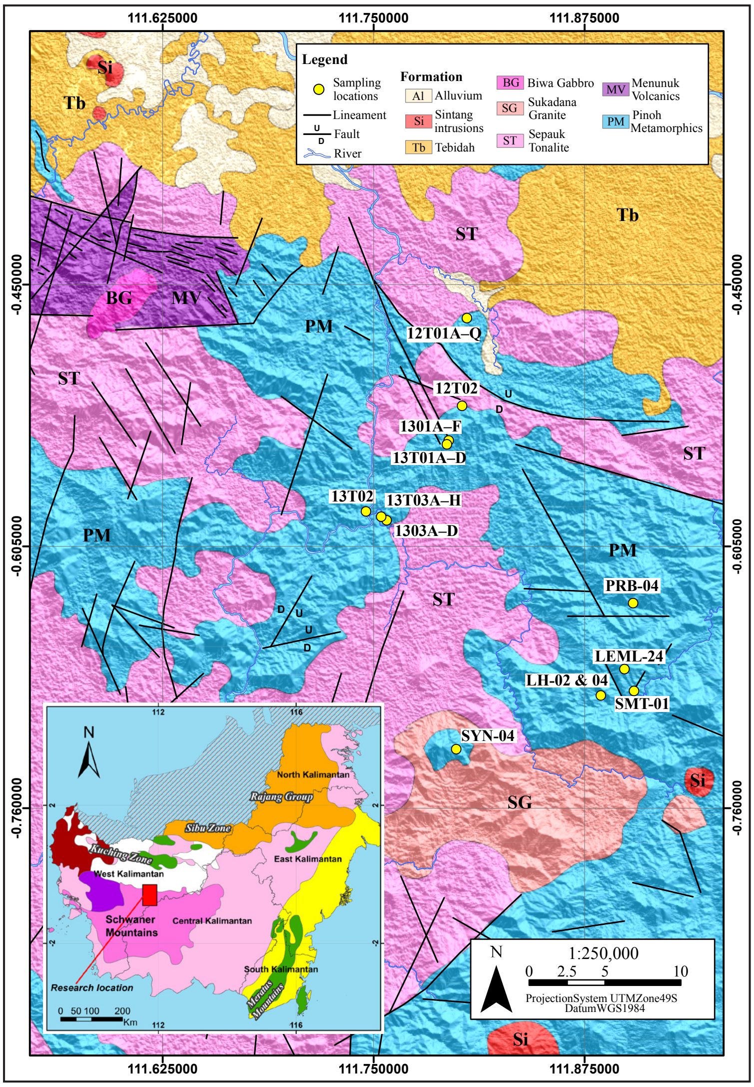

Figure 1. Digital Elevation Model (DEM) (https://tanahair.indonesia.go.id) overlay with a simplified geological map of Nanga Pinoh and Nanga Semalam areas in the Schwaner Mountains region (modified from Amirrudin and Trail, 1993). Surface outcrop sampling locations of metamorphic rocks are indicated on the map. The inset shows the simplified distribution of Cretaceous granitoid and basement units of western and central Kalimantan (modified from Qian et al., 2022).

and Trail, 1993). Foliation developed in the tonalite in contact with the metamorphic rocks, referred to as metatonalite (Amiruddin and Trail, 1993). The schistosity of the metatonalites generally ranges from E-W to NE-SW (Amiruddin and Trail, 1993). The metamorphic rocks were initially interpreted as the Permo-Carboniferous basement of Southwest Borneo (e.g., Bemmelen, 1949) or Palaeozoic to Triassic (*e.g.* Amiruddin and Trail, 1993). A single whole-rock K-Ar age of 189 ± 2 Ma from a biotite hornfels was reported by Mouret in Blandon *et al*. (1989). Davies *et al*. (2014) reported Early Cretaceous U-Pb zircon ages for these metamorphic rocks. More recently, Breitfeld *et al*. (2020) identified two significant metamorphic peaks in the Pinoh metamorphic rocks: the first peak, around 120-110 Ma, is interpreted as thermal metamorphism due to the intrusion of The Sepauk Tonalite, while the second peak, around 90-80 Ma, is associated with later magmatic intrusions.

Methods and Materials

Methods

The major, trace, and rare-earth element compositions of the metamorphic rock samples were analyzed by X-ray fluorescence spectrometry (XRF) using Rigaku ZSZ Primus II and by laser ablation-inductively coupled plasma-mass spectrometry (LA-ICP-MS) with an Agilent 7500cx quadrupole ICP-MS and a New Wave Research UP-213 laser at Kyushu University, Japan, on a fused glass disk (sample: flux ratio = 1:2). The detailed analytical conditions and procedures are given in Adachi *et al*. (2012).

Mineral chemistry compositions of garnet, biotite, muscovite, andalusite, and chlorite were analyzed using JEOL JXA-ISP100 Super-probe electron probe microanalyzer (EPMA) at the Engineering Research Innovation Centre (ERIC), Faculty of Engineering, Universitas Gadjah Mada, Indonesia. The analytical conditions for EPMA were set to an accelerating voltage of 15 kV, a probe current of 12 nA, and a beam diameter of 1 μm. The instrument was internally calibrated using synthetic and natural mineral standards, including Si (SiO_2), K (orthoclase), Al (Al_2O_3), Fe (hematite), Mg (MgO), Na (albite), Mn (rhodochrosite), Ti (TiO_2), and Ca (wollastonite), derived from reference materials MAC 16704, 15298, and 15299. Raw data were corrected using the ZAF method implemented in JEOL's proprietary software. Mineral compositions were recalculated into atoms per formula unit (apfu) following the recommendation by Deer *et al*. (2013). The Fe^{3+} contents of garnet were calculated using the stoichiometric method proposed by Droop (1987).

Pressure-temperature (*P-T*) phase equilibria modeling was performed using pseudosection calculations in the MnNCKFMASH chemical system (MnO-Na_2O-K_2O-FeO-MgO-Al_2O_3-SiO_2-H_2O) with the Perple-X software package (Connolly, 2005) and the internally consistent thermodynamic dataset of Holland and Powell (1998). The bulk-rock composition used for modeling was derived from the whole-rock geochemical data. Mineral solution models used for these calculations were biotite and garnet (White *et al*., 2005), white mica (Coggon and Holland, 2002), and chlorite (Holland and Powell, 1998). Albite, andalusite, and H_2O were considered pure phases. The influence of Fe^{3+} was neglected because of the presence of graphite, which indicated a low oxygen fugacity. The H_2O content was assumed to be saturated throughout the modelled *P-T* range.

Materials

Metamorphic rock samples were collected from surface outcrops in the northern Schwaner Mountains, particularly in the southern Nanga Pinoh and Nanga Semalam areas (Figure 1). A total of forty-two surface outcrop samples were collected during the fieldwork. All collected samples were subjected to petrographic analysis using thin sections to identify mineral assemblages, textures, and rock compositions. From this dataset, three representative metamorphic rock samples (12T01C, 12T01F, and 12T01O) were selected for the whole-rock geochemical analysis based on their freshness, textural clarity, and representativeness of the main lithological variations. Among these, sample 12T01O exhibits the most well-preserved textures and mineralogical assemblages and was therefore further analyzed for microstructural observations and EPMA to constrain mineral chemistry and to determine *P-T* conditions.

Results and Analysis

Field Observation

Samples are Pinoh metamorphic rocks located in the Nanga Pinoh and Nanga Semalam areas (Figure 1) that occur near the contact with the granitoid body, suggesting that the rocks may have undergone contact metamorphism. Field observations were conducted in hilly terrain characterized by dense tropical rainforest vegetation, resulting in generally scarce, discontinuous rock exposure. Outcrops are challenging to access and are mainly found along river cliffs and road cuts, with road-cut exposures providing clearer and more continuous sections than natural riverbank outcrops. In general, most outcrops have undergone significant surface weathering due to prolonged exposure in a tropical rainforest environment. Weathered surfaces commonly display reddish to brownish colours (Figure 2), interpreted as the result of intense chemical weathering and oxidation. Relatively fresh samples were obtained from the inner parts of outcrops or by breaking rocks to expose unweathered cores.

Some rocks still preserve the original slaty fabric with E-W and NW-SE foliation directions, approximately striking from N 88°E to N 130°E, with dip variation from 20°S to 30°S. These are consistent with the main structure identified by Amiruddin and Trail (1993) and Setiawan *et al*. (2013). Other outcrops show less or absent foliation, typical of hornfelsic textures, including andalusite-biotite hornfels and epidote-biotite hornfels (Figure 2). The variation of contact metamorphic rocks includes andalusite-biotite schist (Figures 2a-b), cordierite-andalusite-biotite schist, and biotite-epidote hornfels (Figures 2c-d). Plutonic rocks observed in this location are granite, biotite tonalite, and gabbro, which are possibly recognized as Sepauk Tonalite, Sukadana Granite, and Biwa Gabbro (*e.g.* Amirrudin and Trail, 1993; Hennig *et al*., 2017).

Petrography

Petrographic analyses of forty-two surface outcrop samples reveal a diverse assemblage of contact metamorphic rocks, dominated by schistose and hornfelsic lithologies (Table 1). Mineral abbreviations follow Whitney and Evans (2010). The rocks are generally quartz-rich and characterized by variable proportions of aluminous minerals, reflecting differences in bulk composition, metamorphic grade, and local deformation intensity.

Figure 2. Representative field photographs from the studied area showing the main metamorphic rock lithologies. (a) Andalusite-biotite schist outcrop in the Nanga Pinoh area. (b) Andalusite-biotite hornfels outcrop in the Nanga Pinoh area. (c) and (d) Biotite-epidote hornfels outcrops in the Nanga Semalam area.

Table 1. Mineral Assemblages of Metamorphic Rocks in The Schwaner Mountains. Mineral abbreviations after Whitney and Evans (2010)

Sample No.	Rock Type	Crd	Grt	And/ Chi	Fi/ Sil	Bt	Ms	Qz	Chl	Ep	Gr	Opq	Ap
12T01C; 1301F; 13T01C; 13T01B; 12T01L; 12T01N; 12T02; SYN-04; PRB-04	Crd-And-Bt schist	++	–	++	+	++	+	++	++	–	o	o	o
12T01D; 12T01F; 12T01G; 12T01L; 12T01I; 12T01M; 12T01Q	Crd-Fi (Sil)-And-Bt schist	++	–	++	++	++	+	++	o	–	o	o	o
13T03C; 13T03A; 12T01K; 12T01A; 12T01J; 1301B; 1301D; 1303C	Chi (And)-Bt schist	–	–	++	–	++	+	++	o	–	o	o	o
12T01B; 12T01H; 13T01E; 1301E; 1303A; 1303B; 13T01D; 13T03D; 13T03B	And-Bt schist	–	–	++	–	++	+	++	+	–	o	o	o
12T01E; 1302; LH-04	And-Bt hornfels	–	–	++	–	++	o	++	+	–	o	o	o
13T03F; 12T01O; 13T03G	Grt-And-Bt schist	–	+	++	–	++	o	++	+	–	o	o	o
LH-02; LEML-24; SMT-01	Ep-Bt hornfels	–	–	–	–	++	o	++	+	++	–	o	o

(++) = phase present > 10 %; (+) = phase present 1–10 %; (o) = phase present <1 %; (–) = not present

Cordierite-andalusite-biotite schist

This lithology is represented by samples 12T01C, 13T01F, 13T01B, 12T01L, 12T01N, 12T02, SYN-04, and PRB-04 (Table 1). These rocks are characterized by abundant cordierite and andalusite (>10%), accompanied by biotite (1-10%) and subordinate fibrolite/sillimanite, with quartz and muscovite forming a major part of the matrix (>10%). Accessory graphite and apatite are locally present. The rocks commonly display a schistose to weakly foliated fabric, defined by the preferred orientation of biotite and fibrolitic sillimanite (Figure 3a). Andalusite typically occurs as subhedral to idioblastic porphyroblasts, approximately 0.5-1 mm in size, and locally exhibits poikiloblastic textures. Cordierite forms anhedral grains within the quartz-rich matrix and is locally altered to fine-grained mica or chlorite along grain margins. Fibrolite occurs as scarce, dark, acicular aggregates elongated intergranularly within quartz or forming fibrolite-rich layers in the matrix (Figure 3a). Garnet is absent from this assemblage, suggesting relatively low-pressure metamorphic conditions.

Cordierite-fibrolite (sillimanite)-andalusite-biotite schist

Samples 12T01D, 12T01F, 12T01G, 12T01L, 12T01M, and 12T01Q belong to this assemblage. These rocks are distinguished by the co-existence of cordierite, andalusite, and fibrolite/sillimanite, all present in abundance exceeding 10%, with biotite in moderate amounts and quartz-muscovite forming a significant matrix (Figure 3b). Schistosity in these rocks is generally weak and locally absent, with granoblastic textures predominating. Cordierite and andalusite occur as porphyroblasts (0.5-1 mm) embedded in a quartz-rich matrix. Fibrolite occurs mainly as fine acicular aggregates intergrown with biotite and muscovite, locally defining prograde growth during heating. Secondary minerals such as sericite, pinite, and chlorite locally replace andalusite, cordierite, biotite, and muscovite, reflecting retrograde alteration.

Chiastolite (andalusite)-biotite schist

This assemblage includes samples 13T01C, 13T03A, 12T01K, 12T01A, 12T01J, 13T01B, and 13T01D. These rocks are characterized by abundant chiastolite together with biotite, quartz, and muscovite, whereas cordierite and garnet are absent. The rocks exhibit a fine- to medium-grained schistose texture, with foliation defined by aligned biotite and muscovite. Andalusite commonly occurs as prismatic to poikiloblastic crystals, locally displaying well-developed chiastolitic textures, marked by abundant graphite and quartz inclusions that form a characteristic

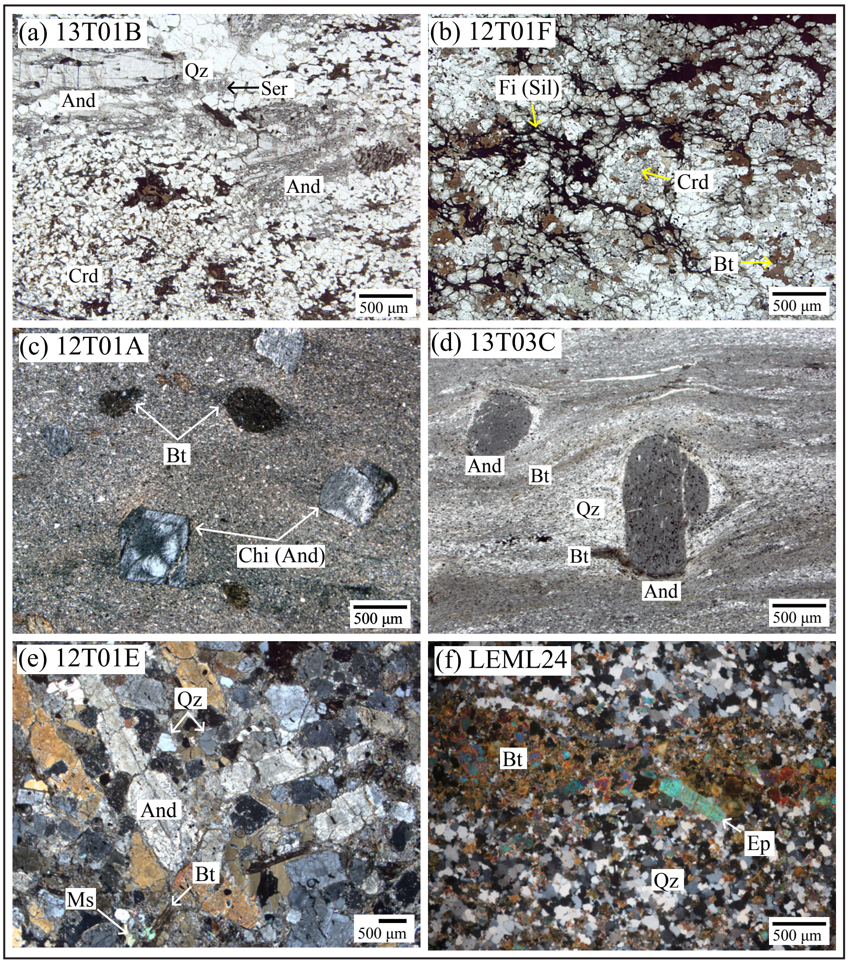

Figure 3. Representative photomicrographs of Pinoh metamorphic rocks in The Schwaner Mountains (plane-polarized and crossed-polarized light). (a) Cordierite-andalusite-biotite schist (sample 13T01B) showing porphyroblastic andalusite embedded in a quartz-rich matrix and anhedral cordierite. (b) Cordierite-fibrolite (sillimanite)-biotite schist (sample 12T01F) showing fibrolite intergrown with biotite within a quartz-dominated matrix. (c) Chiastolite (andalusite)-biotite schist (sample 13T03C) displaying characteristic chiastolitic texture and nodular biotite. (d) Andalusite-biotite schist (sample 13T03C) showing augen-shaped andalusite porphyroblasts wrapped by biotite-quartz schistosity. (e) Andalusite-biotite hornfels (sample 12T01E) with granoblastic to decussate textures formed by interlocking andalusite, biotite, quartz, and minor muscovite. (f) Epidote-biotite hornfels (sample LEML-24) is characterized by nematoblastic epidote in a fine-grained quartz matrix. with dispersed biotite.

cross-shaped pattern (Figure 3c). This assemblage indicates relatively lower metamorphic temperatures within the andalusite stability field than in cordierite-bearing schists and is typical of low-pressure contact metamorphism.

Andalusite-biotite schist

Samples 12T01B, 12T01H, 13T01E, 13T03A, 13T03B, 13T01D, and 13T03D are classified as andalusite-biotite schist. These rocks are dominated by andalusite (>10%), biotite, quartz, and muscovite, with minor chlorite locally and common accessory graphite. They display a well-developed schistose fabric, with andalusite occurring as rounded to idioblastic poikiloblasts measuring 1-2 mm (Figure 3d). In several samples, andalusite porphyroblasts show augen-shaped morphologies with quartz-filled pressure shadows, suggesting that deformation postdated peak thermal metamorphism. Muscovite occurs as fine-grained lepidoblastic flakes (<0.1 mm) aligned parallel to the schistosity. Fine-grained garnet is rarely present.

Andalusite-biotite hornfels

Samples 12T01E, 13T02, and LH-04 represent hornfelsic equivalents of the andalusite-biotite assemblage. These rocks are characterized by granoblastic to mosaic textures, weak or absent foliation, and mineral assemblages dominated by andalusite, biotite, quartz, and muscovite. Nematoblastic andalusite crystals (0.5-1 mm) form interlocking or decussate textures (Figure 3e), while biotite commonly occurs as nodular or spotted aggregates of similar size. The absence of penetrative foliation and the equigranular texture indicate static recrystallization under contact metamorphic conditions.

Epidote-biotite hornfels

Samples LH-02, LEML-24, and SMT-01 are classified as epidote-biotite hornfels. These rocks have a simple mineral assemblage dominated by epidote, biotite, and quartz, with or without plagioclase (Figure 3f), and show weak foliation. Epidote occurs as nematoblastic crystals (~0.5 mm) with greenish to brownish colours and high relief, embedded in a fine-grained quartz matrix. Fine-grained biotite flakes (~0.1 mm) are dispersed throughout the matrix. The texture and mineral assemblage reflect low- to medium-grade thermal metamorphism, possibly influenced by Ca-rich protolith compositions.

Garnet-andalusite-biotite schist

Samples 13T03F, 12T01O, and 13T03G contain garnet in addition to andalusite, biotite, quartz, and muscovite. Garnet occurs as fine-grained idioblastic porphyroblasts (0.1-0.25 mm), generally in low modal abundance (1-10%), and is commonly associated with nodular biotite (Figures 4a-b). Garnet porphyroblasts are locally wrapped by the schistosity defined by biotite, suggesting syn- to post-kinematic growth. The presence of garnet indicates locally higher pressure or more Fe-rich bulk compositions than in garnet-absent assemblages.

Microstructural Features

A representative sample of garnet-andalusite-biotite schist (sample 12T01O) was selected for microstructure analysis (Figures 4a-b). This rock is composed of biotite, quartz, muscovite, andalusite, and garnet, with accessory graphite, apatite, and ilmenite. Chlorite locally occurs as an alteration product of biotite. The microfabric is dominated by the development of a well-developed S_1 foliation, expressed as a straight to gently undulose fabric defined primarily by the preferred alignment of fine-grained muscovite flakes (~0.1 mm). Coarse-grained porphyroblastic biotite and andalusite (0.5-1 mm) are present and are broadly aligned parallel to the S_1 foliation. Inclusion trails of quartz, muscovite, graphite, and ilmenite within coarse-grained biotite are consistently oriented parallel to the external S_1 foliation.

Idioblastic, fine-grain garnet (0.1-0.3 mm) occurs in low modal abundance (~3%) and is commonly in contact with porphyroblastic biotite. Garnet grains are inclusion-free and display homogeneous composition, with no significant chemical zoning observed (see Mineral Chemistry section). A later crenulation cleavage (S_2) overprints the S_1 foliation and is developed in all major mineral phases, including muscovite, biotite, and andalusite. The S_2 fabric is expressed as closely spaced shear-related microfolds and crenulations with typical spacings of approximately ~1 mm, locally deflecting the earlier S_1 foliation.

Geochemistry

Three representative samples of Pinoh metamorphic rocks were analyzed for whole-rock geochemistry using XRF and ICP-MS techniques. These samples include garnet-andalusite-biotite schist (12T01O), cordierite-andalusite-biotite schist (12T01C), and andalusite-biotite schist (12T01F). The geochemical data, including major, rare-earth, and trace elements, are presented in Table 2.

The analyzed samples are characterized by moderate to high SiO_2 contents (60.02-67.73 wt.%) and elevated Al_2O_3 concentrations (16.57-22.00 wt.%), typical of metapelitic compositions. Fe_2O_3 (5.88-7.13 wt. %), MgO (1.32-1.66 wt. %), and MnO (0.07-0.09 wt. %) contents are relatively uniform among samples, indicating broadly comparable Fe-Mg bulk compositions. In contrast, CaO (0.24-0.58 wt.%) and Na_2O (0.59-1.05 wt.

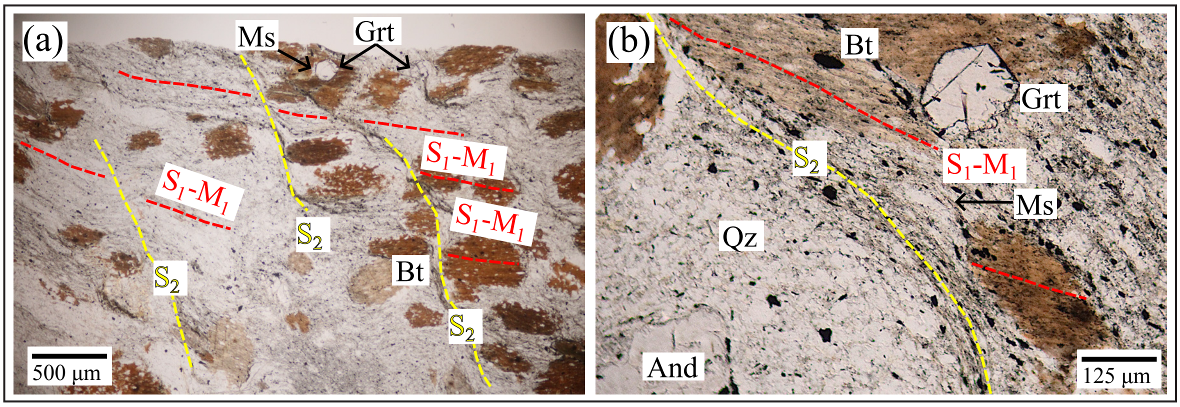

Figure 4. Microstructural features of garnet-andalusite-biotite schist (sample 12T01O). (a) S_1 foliation is defined by aligned muscovite, with biotite and fine-grained garnet occurring parallel to foliation; S_2 crenulation locally overprints S_1. (b) Close-up showing S_2 crenulation cleavage affecting quartz, muscovite, biotite, and andalusite, locally deflecting the earlier S_1 foliation.

%) contents are consistently low, reflecting substantial feldspar depletion and chemical maturity of the protoliths. Potassium contents (K_2O = 2.60-4.15 wt. %) combined with low K_2O/Al_2O_3 ratios (0.16-0.19) further support derivation from Al-rich, clay-dominated sedimentary precursors. Trace-element abundances show enrichment in large-ion lithophile elements (Rb= 128-215 ppm; Ba= 361-508 ppm) relative to high field strength elements (Nb= 16-20 ppm; Zr= 189-231 ppm). Rare-earth element patterns are characterized by LREE enrichment (La= 39-55 ppm; Ce= 76-106 ppm), and comparatively lower HREE contents, consistent with sedimentary recycling and fractionation processes. The presence of negative Sr anomalies (Sr= 58-115 ppm) suggests plagioclase depletion during source weathering and/or sedimentary sorting.

Overall, the geochemical characteristics of the studied samples closely overlap with those reported for metapelites and hornfels from The Pinoh Metamorphic Rocks by Breitfeld *et al.* (2020), including major-element compositions, trace-element distributions, and weathering indices (Table 2). Minor differences, such as slightly higher SiO_2 contents in sample 12T01C, are interpreted as reflecting local sedimentary heterogeneity or differential enrichment of quartz rather than fundamentally different protolith types.

Elemental concentrations, normalized to the average upper continental crust (UCC) values as reported by Taylor and McLennan (1985), are shown in Figure 5. Overall, the analyzed metapelites display UCC-like trace-element patterns that closely overlap those reported by Breitfeld *et al.* (2020), indicating broadly similar protolith characteristics. Significant ion lithophile elements (LILE) show moderate enrichment in Rb, reflecting the abundance of K-bearing clay minerals and muscovite in the protoliths. In contrast, Ba exhibits slight to moderate depletion, whereas Sr shows pronounced negative anomalies relative to UCC values. The Sr depletion is interpreted to result from significant plagioclase depletion during chemical weathering and sedimentary recycling prior to deposition (Taylor and McLennan, 1985; Nesbitt and Young, 1982).

High field strength elements (HFSE) and rare-earth elements (REE) are generally characterized by slight enrichment to near-UCC levels. Th, La, Ce, and Nd show weak enrichment, consistent with derivation from felsic to intermediate continental crustal sources. Zr concentrations fluctuate around UCC values, suggesting variable contributions from detrital zircon during sedimentary sorting. Heavy REE (Y and Yb) display near-flat to slightly enriched patterns, indicating limited fractionation during sedimentary processes (Taylor and McLennan, 1985). A notable feature of the analyzed samples is the relative enrichment of Sm, which is more pronounced than in metapelitic samples reported by Breitfeld *et al.* (2020). This enrichment may reflect variations in the abundance of REE-bearing accessory minerals

Table 2. The Whole Rock Chemistry of Pinoh Metamorphic Rocks in The Schwaner Mountains

	This Study			**Breitfeld *et al.* (2020)**									
Sample No	**12T01C**	**12T01F**	**12T01O***	**LD09-11SW11**	**LD10-004B**	**LD10-052**	**LD10-056**	**LD10-059**	**LD10-064**	**LD10-065A**	**LD10-066**	**LD10-084**	**LD10-102A**
Rock Type	**Crd-and-Bt schist**	**Crd-Sil (Fi)-and -Bt schist**	**Grt-and-Bt schist**	**and-Crd schist**	**Bt schist**	**Crd-and hornfels**	**Grano-fels**	**and hornfels**	**and-Crd schist**	**Schist**	**and-Crd schist**	**Grt-Sil schist**	**Schist**
SiO_2	67.73	60.02	66.35	58.54	62.90	61.69	62.41	64.82	64.62	63.07	63.43	61.94	66.58
TiO_2	1.02	1.08	0.89	0.89	0.93	0.78	0.81	0.84	0.77	0.98	0.90	0.91	0.75
Al_2O_3	16.57	22.00	17.71	24.38	19.58	21.22	20.64	19.39	19.49	22.01	21.25	21.63	18.39
Fe_2O_3	6.07	7.13	5.88	8.81	6.87	7.93	6.97	7.84	7.67	5.42	7.36	7.34	5.23
FeO	5.46	6.41	5.29	7.93	6.18	7.14	6.27	7.05	6.90	4.88	6.62	6.60	4.71
MnO	0.08	0.07	0.09	0.08	0.10	0.11	0.07	0.14	0.09	0.18	0.09	0.09	0.05
MgO	1.66	1.32	1.59	1.76	1.99	1.64	1.45	1.72	1.65	1.05	1.51	2.01	1.79
CaO	0.24	0.58	0.35	0.63	0.91	0.51	1.47	0.43	0.53	0.24	0.03	0.44	0.31
Na_2O	0.67	1.05	0.59	1.17	1.23	0.87	1.13	0.83	0.81	0.93	0.29	0.48	0.58
K_2O	2.60	4.15	2.88	3.23	2.83	2.95	2.67	2.67	2.64	3.87	2.33	3.14	3.33
P_2O_5	0.07	0.05	0.12	0.09	0.09	0.12	0.08	0.10	0.11	0.06	0.08	0.07	0.05
LOI	2.69	2.10	2.99	-	-	-	-	-	-	-	-	-	-
TOTAL	99.39	99.54	99.44	99.58	97.43	97.82	97.70	98.78	98.38	97.81	97.27	98.05	97.06
V	106.64	127.29	106.45	160.34	135.29	134.85	142.93	131.01	124.83	145.35	138.12	151.26	134.13
Cr	132.58	139.92	118.15	114.27	94.62	85.17	84.27	88.96	81.54	92.30	102.71	103.47	91.65
Co	320.03	65.56	215.26	36.05	23.21	23.12	28.17	18.51	21.59	10.38	22.77	17.15	32.53
Ni	9.30	49.79	11.57	41.58	38.37	35.14	28.91	34.81	26.08	36.97	43.12	30.21	25.25
Cu	23.46	16.67	18.22	25.84	31.53	24.61	18.90	37.79	12.97	20.36	24.72	27.98	8.77
Zn	84.97	53.95	86.28	144.81	94.00	134.51	102.80	112.73	84.61	47.40	100.96	112.43	84.38
Ga	19.36	25.48	21.03	30.56	24.38	26.36	25.32	23.90	24.68	26.91	26.13	27.01	22.99
Rb	128.64	215.45	156.21	199.57	105.91	206.40	166.80	170.72	192.53	231.42	119.50	181.38	173.78
Sr	58.12	115.44	62.89	123.90	124.20	96.87	140.91	83.17	120.13	88.34	35.85	58.06	102.81
Y	36.95	27.79	34.72	34.01	36.12	32.80	30.42	34.63	34.61	37.47	34.77	33.19	24.14
Zr	230.97	188.51	226.64	182.09	219.74	172.66	188.58	198.25	193.17	194.70	214.55	203.99	157.74
Nb	17.24	19.71	16.15	17.51	18.39	17.50	16.45	16.52	17.96	18.30	18.01	18.77	15.62
Ba	360.92	507.70	386.21	367.39	530.24	273.88	273.15	326.40	262.32	381.25	345.98	372.13	385.38
La	54.50	39.05	43.15	38.07	34.02	36.11	32.55	29.55	35.78	34.38	76.17	33.11	30.91
Ce	106.41	76.42	84.05	75.26	70.69	75.91	72.37	67.31	76.03	70.83	92.24	69.95	50.44
Nd	45.92	34.69	38.14	32.86	31.01	32.99	30.21	28.22	34.04	30.60	52.00	30.55	26.15
Sm	22.39	9.60	16.10	6.53	6.15	7.66	4.53	6.04	5.72	7.54	8.79	6.12	4.76
Pb	6.82	17.79	21.54	32.81	25.81	24.57	27.24	26.59	11.70	6.70	22.67	18.36	19.74
Th	14.09	13.22	15.64	22.10	19.43	21.14	20.76	20.09	18.86	20.39	22.91	21.83	17.55
K_2O/Al_2O_3	0.16	0.19	0.16	0.13	0.14	0.14	0.13	0.14	0.14	0.18	0.11	0.15	0.18
Al_2O_3/-TiO_2	16.24	20.31	19.85	27.39	21.05	27.21	25.48	23.08	25.31	22.46	23.61	23.77	24.52
Cr/Zr	0.57	0.74	0.52	0.63	0.43	0.49	0.45	0.45	0.42	0.47	0.48	0.51	0.58
CIA	82.55	79.21	82.28	82.90	79.76	83.05	79.66	83.15	83.04	81.37	88.91	84.20	81.34
CIW	94.82	93.12	94.97	93.12	90.15	93.89	88.81	93.90	93.57	94.95	98.52	95.92	95.38
ICV	0.74	0.70	0.69	0.68	0.75	0.69	0.70	0.74	0.72	0.57	0.58	0.66	0.65
$100TiO_2/Zr$	0.44	0.57	0.39	0.49	0.42	0.45	0.43	0.42	0.40	0.50	0.42	0.45	0.48

*Data used for pseudosection calculation

(e.g., monazite, apatite) or differential retention of middle REE during sedimentary recycling. Overall, the trace-element and REE characteristics are consistent with those of compositionally mature pelitic protoliths, in which elemental distributions are primarily controlled by clay mineral content and detrital accessory phases (*e.g.* Varga and Szakmány, 2004).

The degree of weathering in the source region significantly influences the chemical composition of terrigenous sedimentary rocks, leading to relative depletion of alkali and alkaline-earth elements and enrichment in Al_2O_3 and TiO_2 (*e.g.* Nesbitt and Markovics, 1980; Grandstaff *et al.*, 1986; Harnois, 1988). This concept of weathering has also been applied to metapelites, as

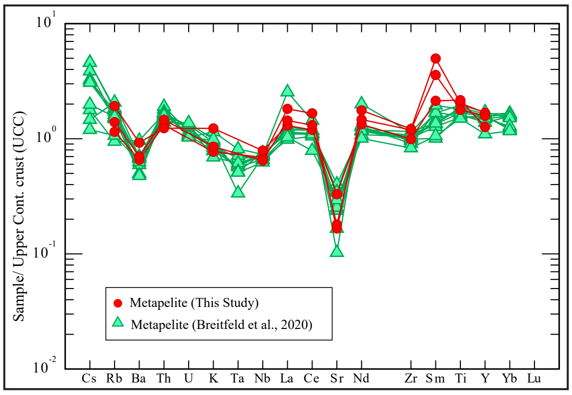

Figure 5. Trace element spider diagram of Pinoh metapelites in the Schwaner Mountains, normalized to the average upper continental crust (UCC) values as reported by Taylor and McLennan (1985).

demonstrated by El-Enen (2011). Weathering intensity can be quantified using the Chemical Index of Alteration (CIA), calculated as CIA= 100 × [Al_2O_3 / (Al_2O_3 + CaO* + Na_2O + K_2O)], where CaO* represents the CaO content exclusively from silicate minerals (Nesbitt and Young, 1982). Another common measure is the Chemical Index of Weathering (CIW), defined as CIW= 100 × [Al_2O_3 / (Al_2O_3 + CaO + Na_2O)] (Harnois, 1988). Typically, unweathered igneous rocks exhibit CIA values below 50, whereas highly weathered rocks, dominated by residual clay minerals, approach CIA values near 100. In this study the CIA values of the analyzed metapelites range from 79.21 to 88.91, while the CIW values span from 88.81 to 98.52. These results suggest that the pelitic sedimentary rock protoliths underwent significant chemical weathering, with CIA values exceeding the average for shales (70-75), as reported by Taylor and McLennan (1985).

Additionally, the Index of Compositional Variability (ICV), proposed by Cox *et al.* (1995) and calculated as ICV= (Fe_2O_3 + K_2O + Na_2O + CaO + MgO + TiO_2) / Al_2O_3, provides insight into the mineralogical maturity of mudrocks in sedimentary basins. Higher ICV values (above 1) are characteristic of immature pelitic rocks, which contain a higher proportion of nonclay silicate minerals, and are typically associated with tectonically active settings (De Kamp and Leake, 1985). Conversely, lower ICV values indicate more mature pelitic rocks enriched in clay minerals, commonly found in tectonically stable or cratonic environments, where sediment recycling and weathering dominate (Weaver, 1989). In the current study (including samples from Breitfeld *et al.*, 2020), ICV values range from 0.58 to 0.75, suggesting that the protoliths of the studied metapelites were derived from mature pelitic rocks that underwent significant chemical weathering in the source region.

The K_2O/Al_2O_3 ratio is a useful indicator of the source composition of fine-grained clastic rocks (Cox *et al.*, 1995). This is based on the variability in K_2O/Al_2O_3 ratios observed between clay minerals (<0.3) and alkali feldspars (0.4-1.0). Cox *et al.* (1995) proposed an empirical threshold of K_2O/Al_2O_3= 0.5 to distinguish between significant and minimal alkali feldspar contributions in the parent rocks of pelites. The average K_2O/Al_2O_3 ratio of the studied metapelites is 0.15, ranging from 0.13 to 0.19 (Table 2), suggesting minimal alkali feldspar content in their protoliths. This indicates that the source rocks were not entirely felsic.

Girty *et al.* (1996) employed the Al_2O_3/TiO_2 ratio to discriminate between source rock compositions, with values below 14 indicating sediments derived from mafic rocks and values between 19 and 28 indicating an intermediate igneous source. The Al_2O_3/TiO_2 ratios for the studied metapelites range from 16.24 to 27.39, with an average of 23.10, suggesting that the precursors of these pelitic sediments were primarily derived from intermediate igneous rocks.

Trace elements, including Cr and Zr, are frequently utilized to infer source rock composition in metapelites (*e.g.* McLennan and Hemming, 1992; Fedo *et al.*, 1995; Cox *et al.*, 1995). Cr and Zr concentrations are often used as proxies for chromite and zircon content, respectively, with the Cr/Zr ratio offering insight into the relative contributions of mafic and felsic sources. The Cr/Zr ratios of the studied metapelites range from 0.42 to 0.74, with an average value of 0.52, reflecting a mixed contribution with felsic contribute more than mafic igneous sources.

ACF and AKF ternary discriminant diagrams from Eskola (1915) and Winkler (1979) constrain the protolith composition of the schists. The investigated schist samples suggest a protolith consisting of pelitic rocks or Al-rich clays and shales, specifically within the greywacke region (Figure 6a). All data, consistently group within a single area on the ACF diagram. However, in the AKF diagram, some samples are dispersed and not plotted within the greywacke region. The investigated schists are also plotted on the log(SiO_2/Al_2O_3) vs. log($Fe_2O_3^{(t)}/K_2O$) discriminant diagram, following Herron (1988). All samples, consistently fall within the shale region,

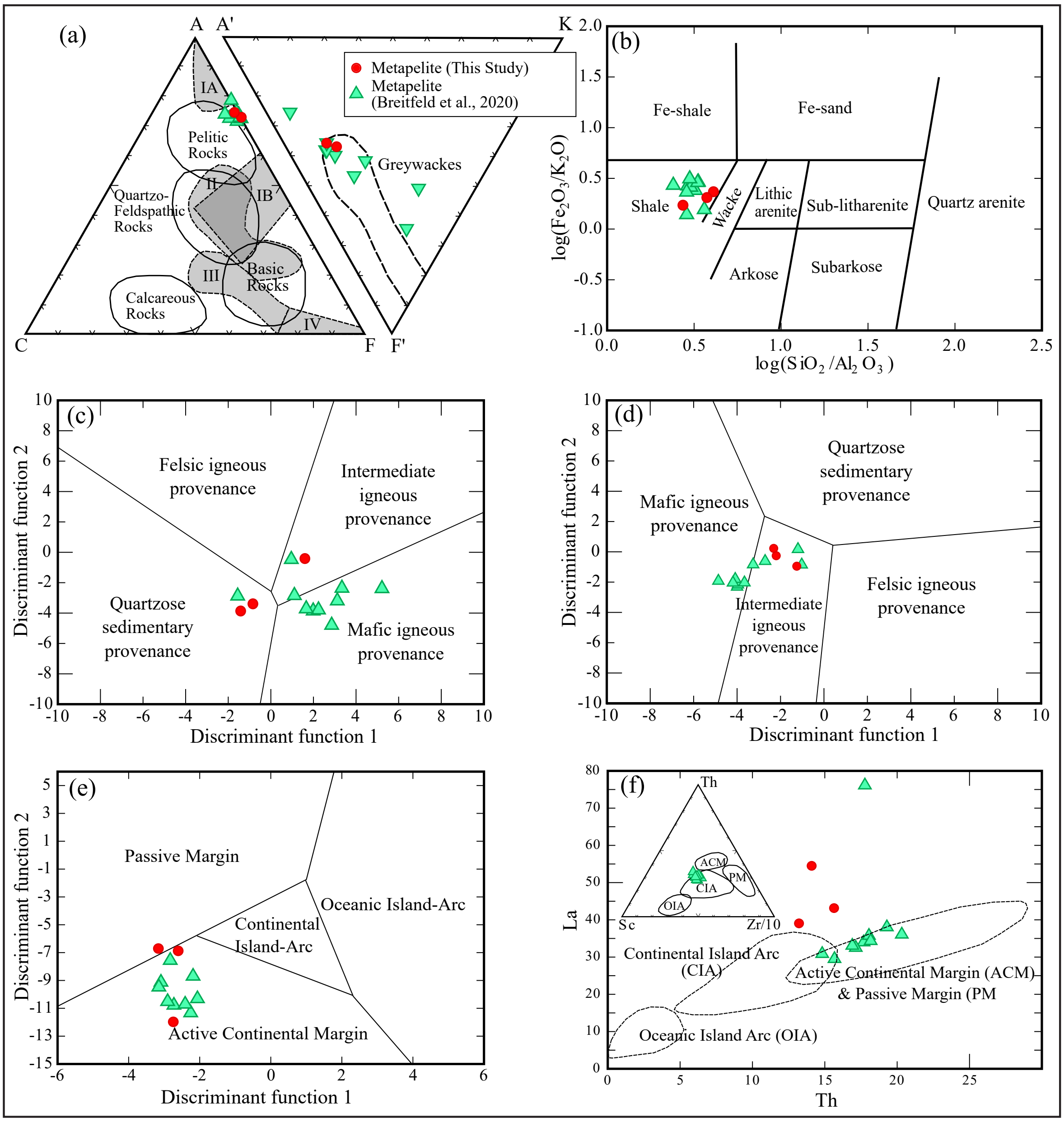

Figure 6. Geochemistry discriminant diagrams of metamorphic rocks from The Schwaner Mountains. (a). ACF and AKF ternary diagram from Eskola (1915) and Winkler (1979) showing fields of IA: Al-rich clays and shales; IB: clays and shales either free of carbonates or containing up to 35 % carbonates; II: greywackes; III: basaltic and andesitic rocks; and IV: ultrabasic rocks; (b) log(SiO_2/Al_2O_3) vs. log($Fe_2O_3^{(t)}/K_2O$) discriminant diagram after Herron (1988); (c, d) Major-element discriminant diagrams and functions after Roser and Korsch (1988). (e) Major-elements discriminant diagram after Bhatia (1993); (f) Th *vs.* La discriminant diagram after Bhatia and Crook (1986), with inset ternary Sc-Th-Zr/10 after Bhatia and Crook (1986).

close to the boundary of the wacke field (Figure 6b). These results align with those obtained using the empirical discrimination ratio 100*TiO_2/Zr (wt.%/ppm) to differentiate psammitic from pelitic sediments (Garcia *et al*., 1991; Häussinger *et al*., 1993), where most of the analyzed samples display values greater than 0.4 (Table 2), indicating derivation from pelitic sediments.

Discriminant diagrams in sedimentary rocks are based on the assumption of a strong relationship between tectonic setting and sedimentary rock provenance. The use of discriminant diagrams should be approached cautiously, as sediment material can be transported from its original tectonic setting into a basin with a different tectonic regime (McLennan *et al*., 1990). The discriminant diagram, using major element combinations and discriminant functions from Roser and Korsch (1988), shows that the studied metapelites are predominantly associated with intermediate and mafic igneous provenance (Figures 6c-d), although a small number (three samples) fall within the quartzose sedimentary provenance area (Figure 6c). The discriminant diagram from Roser and Korsch (1988) for Figure 6c follows the discriminant function 1: -1.773TiO_2 + 0.607Al_2O_3 + 0.76$Fe_2O_{3(total)}$ - 1.5MgO + 0.616CaO + 0.509Na_2O - 1.224K_2O - 9.09 and discriminant function 2: 0.445TiO_2 + 0.07Al_2O_3 - 0.25$Fe_2O_{3(total)}$ - 1.142MgO + 0.438CaO + 1.475 Na_2O + 1.426K_2O - 6.861. While discriminant diagram in the Figure 6d follow the discriminant function 1: 30.638TiO_2/ Al_2O_3 - 12.541$Fe_2O_{3(total)}$/ Al_2O_3 + 7.329MgO/ Al_2O_3 + 12.031Na_2O/ Al_2O_3 + 35.412K_2O/ Al_2O_3 - 6.382 and discriminant function 2: 56.5TiO_2/ Al_2O_3 - 10.879$Fe_2O_{3(total)}$/ Al_2O_3 + 30.875MgO/ Al_2O_3 - 5.404Na_2O/ Al_2O_3 + 11.112K_2O/ Al_2O_3 - 3.89.

The discriminant diagram with major element combinations from Bhatia (1993) suggests that the pelitic protolith of the investigated schists was deposited in an active continental margin (Figure 6e). This discriminant diagram from Bhatia (1993) follows the discriminant function 1: -0.0447SiO_2 - 0.972TiO_2 + 0.008Al_2O_3 - 0.267Fe_2O_3 + 0.208FeO - 3.082MnO + 0.14MgO + 0.195CaO + 0.719Na_2O - 0.032K_2O + 7.51P_2O_5 + 0.303 and discriminant function 2: -0.421SiO_2 + 1.988TiO_2 - 0.526Al_2O_3 - 0.551Fe_2O_3 - 1.61FeO + 2.72MnO + 0.881MgO - 0.907CaO - 0.177Na_2O - 1.84K_2O + 7.244P_2O_5 + 43.57. This finding aligns with the Th vs. La discriminant diagram from Bhatia and Crook (1986), which shows a dominant presence of samples in the active continental margin (ACM) and passive margin (PM) areas. However, a few samples are located outside these regions (Figure 6f). Furthermore, the ternary diagram of Sc-Th-Zr/10 from Bhatia and Crook (1986) confirms that all samples from Breitfel *et al*. (2020) are located in the continental island arc (CIA) field (inset in Figure 6f).

Mineral Chemistry

A garnet-andalusite-biotite schist sample (sample 12T01O) was analyzed to determine its mineral composition using an electron probe microanalyzer (EPMA) at Universitas Gadjah Mada, Indonesia. The analysis conditions and sample standards are detailed in the methodology section. This sample was selected due to its complete mineral composition compared to other metapelite samples (Table 1 and Figures 4a-b), making it suitable for *P-T* estimation using reliable geothermometers and pseudosections. The mineral compositions analyzed include garnet, biotite, muscovite, andalusite, as well as chlorite, with representative data provided in Table 3.

Garnet in this rock is relatively rare, accounting for approximately 3 % of the total mineral composition, and occurs as fine grains measuring 0.1-0.25 mm. The garnet displays an idioblastic to hypidioblastic granular shape, and occurs in contact with biotite and muscovite (Figure 7a). A compositional profile from rim to rim (rim-mantle-core-mantle-rim; Figure 7b) reveals variations in spessartine [X_{Sps} = Mn/(Mn + Mg + Ca + Fe^{total})], grossular [X_{Grs} = Ca/(Mn + Mg + Ca + Fe^{total})], almandine [X_{Alm} = Fe^{total} /(Mn + Mg + Ca + Fe^{total})], and pyrope [X_{Prp} = Mg/(Mn + Mg + Ca + Fe^{total})]. The profile indicates overall chemical homogeneity with only slight core-to-rim zoning and no sharp compositional boundaries between

Table 3. Representative Data of Mineral Chemistry from Garnet-andalusite-biotite Schist (sample 12T01O)

Rock Type	Grt			Bt		Ms		And		Chl	
Position	rim*	mantle	core*	matrix*	matrix	matrix	matrix	matrix	matrix	matrix	matrix
SiO_2	33.88	34.94	34.86	33.99	32.71	48.09	45.92	36.63	37.37	27.51	26.85
TiO_2	0.07	0.07	0.02	1.46	1.70	0.42	0.39	0.04	0.00	1.23	0.88
Al_2O_3	18.81	19.69	19.12	19.92	19.45	34.06	35.40	61.44	62.34	20.23	20.68
FeO	29.29	29.90	30.29	25.07	25.96	1.01	1.53	0.17	0.20	29.95	30.52
MnO	16.74	15.39	15.28	0.37	0.32	0.05	0.06	0.04	0.00	0.40	0.46
MgO	0.73	1.04	1.04	5.90	6.01	0.27	0.32	0.00	0.04	7.38	7.71
CaO	0.80	0.01	0.59	0.00	0.00	0.00	0.08	0.00	0.00	0.02	0.01
Na_2O	0.00	0.00	0.00	0.00	0.00	0.00	0.00	0.00	0.00	0.00	0.00
K_2O	0.03	0.00	0.00	10.68	9.34	13.05	13.13	0.01	0.00	3.61	2.96
Total	100.34	101.04	101.20	97.39	95.49	96.94	96.82	98.33	99.95	90.32	90.07
O	12	12	12	11	11	11	11	20	20	28	28
Si	2.87	2.90	2.90	2.63	2.58	3.17	3.06	4.02	4.04	5.86	5.74
Ti	0.00	0.00	0.00	0.08	0.10	0.02	0.02	0.00	0.00	0.20	0.14
Al	1.88	1.93	1.88	1.81	1.81	2.65	2.78	7.95	7.94	5.08	5.21
Fe	2.07	2.08	2.11	1.62	1.71	0.06	0.08	0.02	0.02	5.34	5.46
Mn	1.20	1.08	1.08	0.02	0.02	0.00	0.00	0.00	0.00	0.07	0.08
Mg	0.09	0.13	0.13	0.68	0.71	0.03	0.03	0.00	0.01	2.35	2.46
Ca	0.07	0.00	0.05	0.00	0.00	0.00	0.01	0.00	0.00	0.00	0.00
Na	0.00	0.00	0.00	0.00	0.00	0.00	0.00	0.00	0.00	0.00	0.00
K	0.00	0.00	0.00	1.05	0.94	1.10	1.11	0.00	0.00	0.98	0.81
Total cation	8.19	8.13	8.16	7.91	7.88	7.03	7.09	12.00	12.00	19.89	19.91
Prp (%)	2.91	8.52	3.83								
Alm (%)	56.65	67.78	56.53								
Sps (%)	9.11	0.15	8.77								
Grs (%)	31.33	23.55	30.87								
XMg				0.30	0.29	0.32	0.27				
XSi				0.59	0.59	0.55	0.52				
XFe				0.70	0.71	0.68	0.73				

*Data used for the calculation of peak *P-T* condition.

the core and mantle. The garnet core to mantle shows relatively higher almandine and pyrope contents and lower spessartine and grossular contents (X_{Alm}: 0.620-0.631, X_{Sps}: 0.312-0.329, X_{Grs}: 0.015-0.027, and X_{Prp}: 0.033-0.039) compared to the rim (X_{Alm}: 0.603-0.626, X_{Sps}: 0.314-0.349, X_{Grs}: 0.021-0.027, and X_{Prp}: 0.027-0.036). Chemical mapping of a representative garnet reveals that it is nearly homogeneous in composition and lacks inclusions (Figures 7c-f).

Biotite exhibits a nodular or spotted texture, with grain sizes ranging from 0.2 to 0.5 mm (Figures 4a-b and 7a). It occurs in contact with garnet and muscovite and contains inclusions of quartz and ilmenite. In some areas, biotite is locally replaced by chlorite along its cleavage planes. The biotite shows an X_{Mg} ratio [Mg/(Mg + Fe)] between 0.27 and 0.31 and an X_{Si} ratio [Si/(Si + Al)] between 0.588 and 0.591 (Figures 7g-h), indicating a homogeneous composition.

Muscovite is identified as flaky, thin, and short, displaying a lepidoblastic texture with grain sizes <0.1 mm (Figures 4a-b and 7a). It frequently occurs in contact with biotite, garnet, and quartz aggregates in the matrix. Muscovite adjacent to biotite and garnet has an X_{Mg} ratio of 0.27-0.32 and X_{Si} of 0.52-0.55, most likely indicating a homogeneous composition.

Andalusite, typically xenoblastic in texture, ranges in size from 0.2 to 0.5 mm. The colourless andalusite within the matrix has an X_{Si} value of 0.336-0.337 (Figures 4a-b). Chlorite is observed replacing biotite along the cleavage (Figure 7a) with X_{Fe} values [Mg/(Mg + Fe^{2+})] ranging from 0.69 to 0.70.

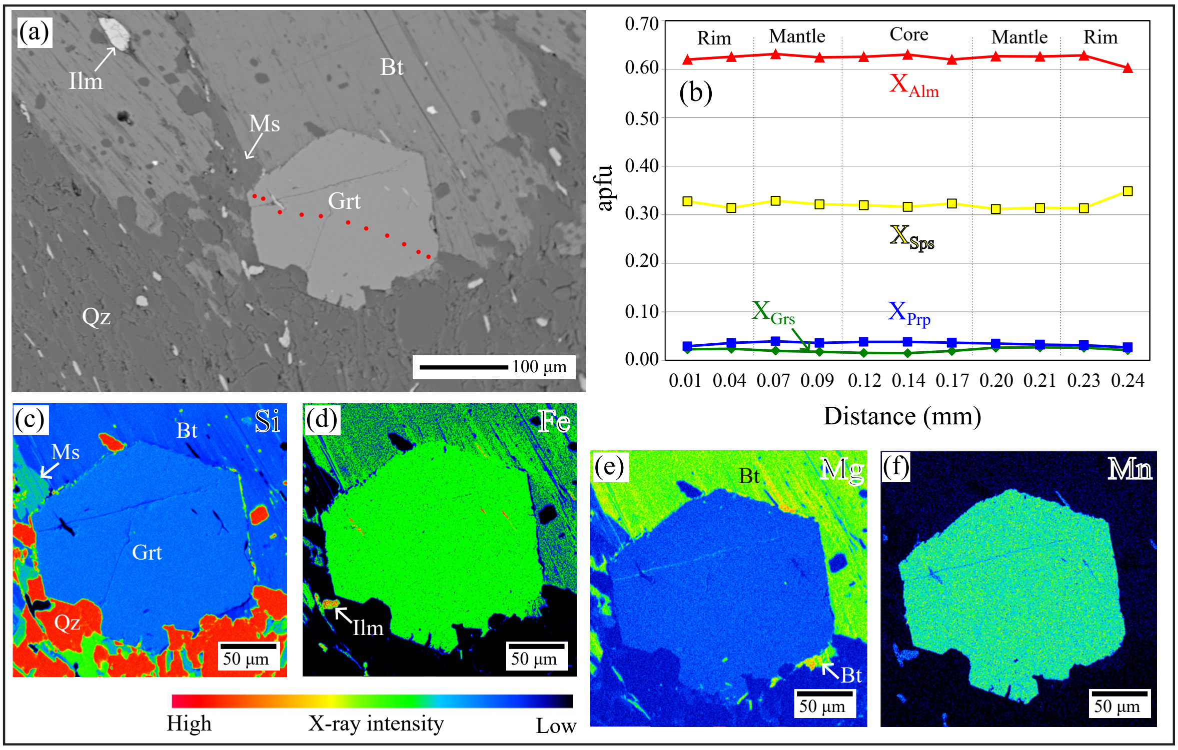

Figure 7. Mineral chemistry analyses of selected sample garnet-andalusite-biotite schist (sample 12T01O). (a) Backscattered image of adjacent garnet and biotite, with other muscovite, quartz, and ilmenite minerals. (b) Compositional profile of representative garnet from rim to rim. (c)–(f) Compositional X-ray maps in the garnet for Si, Fe, Mg, and Mn.

Discussion

Protolith of The Pinoh Metamorphic Rocks

The whole-rock geochemical data from the studied metapelites indicate that the dominant protoliths of the Pinoh Metamorphic Rocks are compositionally mature pelitic to semipelitic sediments. These rocks are characterized by high Al_2O_3 contents, low CaO and Na_2O concentrations, low K_2O/Al_2O_3 ratios, high CIA and CIW values, and low ICV (Table 2). Such geochemical signatures indicate intense chemical weathering, significant sedimentary recycling, and derivation from compositionally evolved sedimentary sources prior to metamorphism. Trace-element and REE patterns normalized to the upper continental crust pronounced LREE enrichment, negative Sr anomalies, and variable Zr contents (Figure 5; Table 2). These features indicate sedimentary sorting, feldspar depletion, and zircon enrichment during sedimentary recycling. Provenance discrimination diagrams consistently suggest derivation predominantly from intermediate- to felsic-igneous sources, with subordinate mafic contributions, deposited in an active continental margin to continental arc setting (Figure 6).

Petrographic observations further indicate that the protolith composition was not uniform across the studied area. The majority of foliated schists (*e.g.* andalusite-biotite schist, garnet-andalusite-biotite schist, cordierite-bearing schists; Table 1; Figures 3a-e) are interpreted to derive from Al-rich pelitic sediments, consistent with their quartz-muscovite-biotite-andalusite ± garnet mineral assemblages. In contrast, epidote-biotite hornfels (Figure 3f) locally preserves Ca-bearing mineral assemblages, suggesting derivation from more Ca-rich protoliths, such as impure pelites, calcareous mudstones, or volcaniclastic sediments with higher plagioclase or carbonate components. The presence of epidote in these lithologies therefore reflects primary bulk-rock compositional control rather than solely metamorphic grade.

These compositional variations of the protolith exerted a first-order control on the metamorphic mineral assemblages and microstructural development during subsequent metamorphic events. Al-rich pelitic protoliths preferentially developed penetrative foliation and aluminous mineral assemblages during regional metamorphism and were later overprinted by andalusite- and cordierite-bearing assemblages during contact metamorphism (Figures 3a-d). In contrast, Ca-bearing protoliths responded to thermal metamorphism primarily through static recrystallization, producing hornfelsic textures without preserving an earlier regional fabric (Figures 3e-f). This distinction provides an important framework for interpreting the spatial distribution of schistose versus hornfelsic lithologies and for evaluating equilibrium mineral assemblages used in *P-T* estimation.

These geochemical characteristics of the studied rocks are broadly consistent with previous interpretations of the Pinoh Metamorphic Group (PMG). Breitfeld *et al.* (2020) proposed that the PMG protoliths represent volcaniclastic sediments equivalent to the Menunuk Volcanics (Figure 1), based on similarities in trace-element spidergrams and the predominance of Early Cretaceous detrital zircons (135-110 Ma). The data support a volcaniclastic contribution, but also indicate a higher degree of compositional maturity and sedimentary recycling, suggesting additional contributions from older, more evolved sedimentary sources (Figure 6). The presence of Triassic to Precambrian detrital zircon populations reported by Breitfeld *et al.* (2020) is consistent with sediment supply from surrounding continental fragments, such as the Karimunjawa Arch, Bird Head, and West Borneo (*e.g.* Witts *et al.*, 2012; Gunawan *et al.*, 2012; Hennig *et al.*, 2017).

Microstructural and Mineralogical Evolution of Metamorphism

Microstructural and petrographic observations of the Pinoh metapelites indicate a polymetamorphic history involving two main metamorphic events, M_1 and M_2, associated with distinct deformation stages and mineral growth patterns (Figure 4). The M_1 event is recorded by the development of a penetrative foliation (S_1), defined primarily by the preferred alignment of muscovite and biotite. This foliation forms a straight to weakly undulose fabric and represents the earliest recognizable metamorphic structure in the studied schists. Mineral assemblages associated with S_1 are dominated by muscovite, quartz, and biotite, with garnet occurring locally as a minor phase. Garnet related to this stage is fine-grained, idioblastic, and volumetrically subordinate (~3 %), suggesting growth during the later stages of M_1 under regional metamorphic conditions.

The M_2 event is characterized by thermal overprinting and is marked by the growth of andalusite porphyroblasts, spotted or recrystallized biotite, and locally garnet (Figure 4). These minerals commonly overgrow or are aligned parallel to the pre-existing S_1 foliation, indicating that M_2 occurred after the development of S_1 and did not generate a new penetrative fabric. The absence of newly developed foliation and the presence of granoblastic to decussate textures in some lithologies (Figure 3) indicate that M_2 was dominantly static and are interpreted as reflecting contact metamorphism associated with a granitoid intrusion.

Garnet observed in the garnet-andalusite-biotite schist is interpreted to have nucleated during the late stage of M_1, but subsequently re-equilibrated during M_2. This interpretation is supported by the fine-grained, idioblastic shape, lack of inclusion trails, and the absence of significant chemical zoning (Figure 7). These features suggest effective Fe-Mg diffusion and chemical homogenization at high temperatures associated with M_2, allowing garnet to participate in mineral equilibrium during the contact metamorphic event.

A later deformational episode (D_2) is recorded by the development of a crenulation cleavage (S_2), which overprints and locally deflects the earlier S_1 foliation (Figure 4). The S_2 fabric affects all major mineral phases, including muscovite, biotite, and andalusite, indicating that deformation occurred after the peak metamorphic conditions of M_2 during cooling. No new metamorphic mineral assemblages are associated with this stage.

The expression of polymetamorphism varies among lithologies. Foliated metapelites, particularly garnet-andalusite-biotite schist and andalusite-biotite schist, preserve both the early regional fabric (S_1) and the later contact metamorphic overprint (M_2) (Figure 4). In contrast, hornfelsic lithologies such as andalusite-biotite hornfels and epidote-biotite hornfels lack penetrative foliation. They are characterized by granoblastic to decussate textures (Figures 3a-b and 3e-f), indicating that these rocks primarily record the thermal effects of contact metamorphism, without preserving an earlier regional fabric.

Estimation of *P-T* Conditions and Equilibrium Assemblage

The *P-T* conditions of the Pinoh metapelites were constrained using two complementary approaches: conventional mineral geothermobarometry and phase equilibria (pseudosection) modeling in the MnNCKFMASH chemical system. Conventional geothermobarometry provides quantitative *P-T* based on mineral compositions assumed to be in equilibrium. In contrast, pseudosection modeling evaluates the stability fields of mineral assemblages and compositional isopleths as functions of *P-T* conditions, using the whole-rock compositions. The combined application of these methods allows cross-validation of *P-T* estimates, and provides robust constraints on metamorphic conditions.

The metapelitic assemblages in the Schwaner Mountains are dominated by quartz, biotite, muscovite, chlorite, and andalusite, with variable occurrences of garnet, graphite, cordierite, and fibrolite (Table 1). Among the analyzed samples, sample 12T01O (garnet-andalusite-biotite schist) preserves the most suitable mineral assemblage for *P-T* estimation, consisting of garnet, biotite, andalusite, and quartz, with muscovite and chlorite occurring as matrix or secondary phases. Petrographic and mineral-chemical data indicate that these phases were chemically equilibrated during the M_2 contact metamorphic event (Figures 4 and 7). Garnet and biotite in sample 12T01O show homogeneous composition (Figure 7). Garnet displays only minor core-rim compositional variations, with slightly higher almandine and pyrope contents and lower spessartine and grossular contents in the core relative to the rim (Figure 7b). These subtle variations are interpreted as reflecting limited retrograde modification, whereas the overall homogeneity indicates near-equilibrium conditions at elevated temperatures.

The Fe-Mg distribution coefficient (K_D = $(Mg/Fe)^{garnet}/(Mg/Fe)^{biotite}$) calculated from garnet cores, rims, and adjacent biotite shows a narrow range of 0.10 to 0.14, consistent with effective Fe-Mg exchange between garnet and biotite. For geothermobarometric calculations, garnet core compositions were paired with adjacent matrix biotite to estimate the *P-T* conditions recorded by the equilibrium mineral assemblages. *P-T* estimates were obtained using the garnet-biotite-andalusite-quartz (GBAQ) geobarometer of Wu (2017) in combination with the garnet-biotite (GB) geothermometer of Holdaway (2000). These methods employ consistent activity-composition models for garnet and biotite, and are well-suited to andalusite-bearing, plagioclase-poor metapelites. The calculated *P-T* conditions yield temperatures of 577-586º C at 3.7-3.8 kbar, consistent with low-pressure, high-temperature contact metamorphic conditions.

To further evaluate the *P-T* conditions and mineral stability relationships, a pseudosection was constructed for sample 12T01O (garnet-andalusite-biotite schist) over a range of 450-650º C and 1-8 kbar (Figure 8), using whole-rock major-element compositions (Table 2). The pseudosection indicates that the stability field of the assemblage garnet-biotite-muscovite-andalusite-quartz-chlorite spans approximately 475-560º C and 0.2-3.0 kbar (Figure 8a). Garnet X_{Mg} (Mg/Mg+Fe) isopleths were projected onto the pseudosection (Figure 8b), and the measured garnet core X_{Mg} values (0.056-0.059; Table 3) intersect the observed assemblage stability field

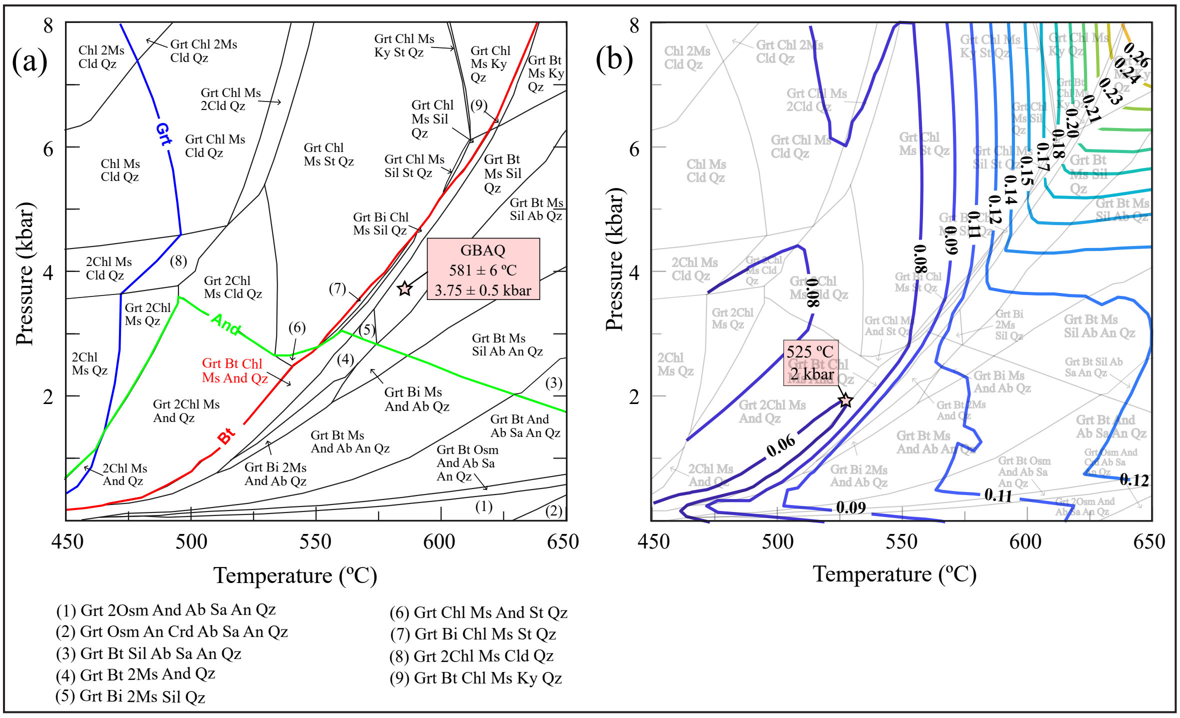

Figure 8. Pseudosection in the MnNCKFMASH system. (a) The pseudosection diagram shows the limit of garnet (blue), andalusite (green), and biotite (red). The *P-T* field of metamorphic assemblages is shown in red. (b) X_{Mg} isopleth of garnet overlays the pseudosection.

at approximately 525º C and 2 kbar (Figure 8b). Taken together, the results from conventional geothermobarometry and phase equilibria modeling constrain peak metamorphic conditions 526-586º C at 2.0-3.8 kbar, consistent with a low-pressure, high-temperature metamorphic regime.

Implications for The Regional Metamorphic History of The Schwaner Mountains

The estimated *P-T* conditions for the Pinoh metapelites (525-586° C at 2.0-3.8 kbar) indicate that metamorphism in the Schwaner Mountains was characterized by low-pressure, high-temperature (LP-HT) conditions, consistent with Buchan-type metamorphism. These conditions are most plausibly related to thermal overprinting associated with granitoid intrusion, rather than to classical regional Barrovian metamorphism or simple, shallow contact aureoles. The absence of syn-metamorphic penetrative deformation during peak heating, together with the development of granoblastic to hornfelsic textures (Figure 3), indicates that the dominant thermal event occurred under largely static metamorphic conditions.

The M_1 event recorded in the Pinoh Metamorphic Rocks is interpreted as an earlier regional metamorphic overprint, responsible for the development of penetrative S_1 foliation and associated muscovite-biotite assemblages in metapelitic schists (Figure 4). Although direct geochronological constraints for M_1 are currently lacking, the preservation of an early foliation and syntectonic mineral growth suggests that regional metamorphism predates granitoid emplacement, consistent with the regional structural and metamorphic frameworks of the Schwaner Mountains (Amiruddin and Trail, 1993; Hennig *et al*., 2017). This event may reflect crustal thickening or burial associated with early tectonic processes in western Kalimantan, prior to widespread Cretaceous magmatism.

In contrast, the M_2 event represents the dominant metamorphic phase preserved in the studied area. It is attributed to thermal input from Cretaceous granitoid intrusions, including the Rantau Asem Tonalite and Sukadana Granite. This interpretation is supported by zircon recrystallization ages of approximately 80-90 Ma reported by Breitfeld *et al*. (2020), which coincide with regional magmatic activity in western and central Kalimantan. The LP-HT conditions inferred from geothermobarometry and pseudosection modeling (Figure 8) are consistent with contact-related Buchan-type metamorphism, characterized by the growth of andalusite ± cordierite and the chemical re-equilibration of earlier-formed minerals, including garnet.

A subsequent deformational phase (D_2) is recorded by the development of crenulation cleavage (S_2), which overprints the earlier S_1 foliation and affects all major mineral phases, including andalusite (Figure 4). The microstructural relationships indicate that this deformation occurred after peak metamorphic conditions of M_2, during cooling and exhumation, rather than during prograde metamorphism. This interpretation is consistent with fine-grained biotite $^{40}Ar/^{39}Ar$ ages of approximately 27 Ma reported by Breitfeld *et al*. (2020), which have been linked to regional uplift, denudation, and strike-slip or transpressional deformation in central Kalimantan during the Late Oligocene (*e.g*. Hall, 2012).

Taken together, the metamorphic evolution of the Pinoh Metamorphic Rocks reflects a polyphase tectono-metamorphic history involving (1) an early regional metamorphic event (M_1) associated with crustal burial and foliation development, (2) a dominant LP-HT Buchan-type metamorphic overprint (M_2) driven by Cretaceous granitoid magmatism under largely static conditions, and (3) a later deformational phase (D_2) related to post-metamorphic tectonic reactivation and exhumation. This evolution highlights the importance of both protolith composition and tectono-magmatic processes in controlling metamorphic styles within the Schwaner Mountains (Figure 9).

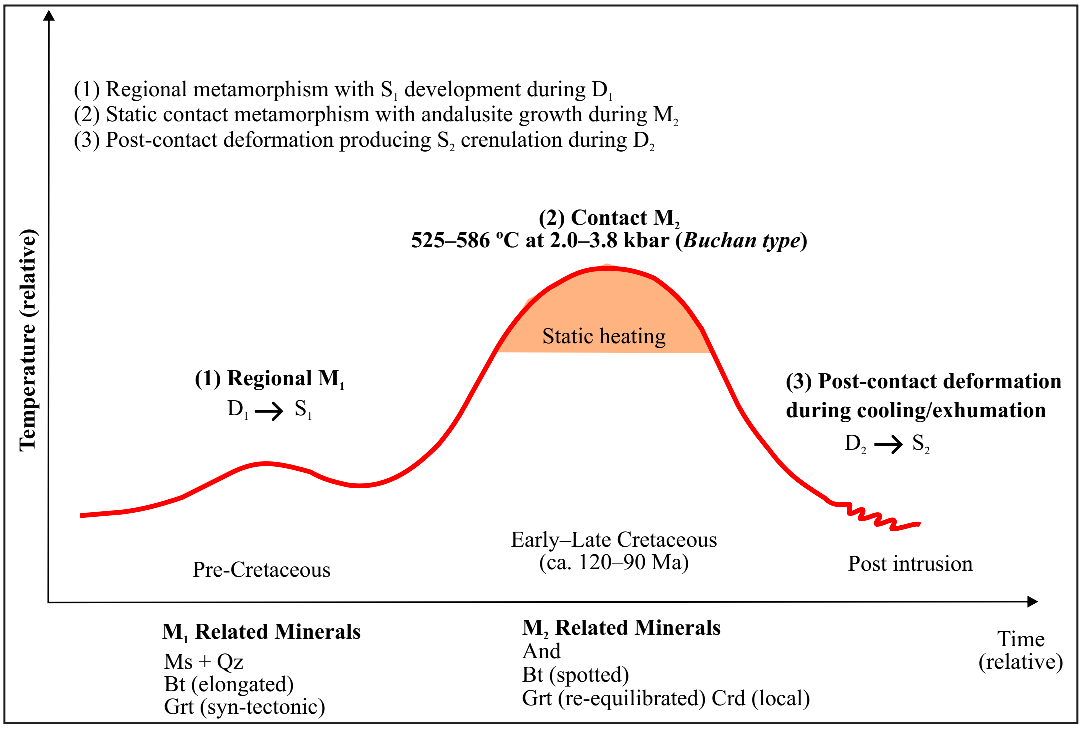

Figure 9. Conceptual temperature–time diagram illustrating the tectono-metamorphic evolution of the Pinoh metamorphic rocks. Regional metamorphism (M_1) with syn-tectonic development of S_1 occurred prior to Cretaceous granitoid intrusion. This was followed by static, low-pressure contact metamorphism (M_2; 525–586° C, 2–3.8 kbar; Buchan-type), during which andalusite grew, and garnet underwent chemical re-equilibration. Subsequent deformation (D_2) produced S_2 crenulation cleavage during post-peak cooling and exhumation.

Conclusion

The protolith of the Pinoh metamorphic rocks is interpreted to consist predominantly of compositionally mature pelitic to semipelitic sediments, derived largely from reworked volcaniclastic material related to the Menunuk Volcanics, with additional contributions from older, more compositionally evolved sedimentary sources. Local occurrences of epidote-biotite hornfels indicate the presence of Ca-rich volcaniclastic or felspathic protolith, highlighting significant compositional heterogeneity within the sedimentary succession. Geochemical characteristics and provenance discrimination consistently indicate deposition in an active continental margin to continental arc setting.

Macro- and microstructural observations record a polyphase metamorphic history involving two main metamorphic events (M_1 and M_2) and at least two deformation stages. The M_1 event is associated with the development of a penetrative S_1 foliation defined by aligned muscovite and biotite, and represents an early regional metamorphic overprint. Garnet locally nucleated during the late stages of M_1 as a minor phase. The M_2 event constitutes the dominant metamorphic overprint. It is characterized by thermal recrystallization and the growth of andalusite porphyroblasts, spotted biotite, with mineral assemblages that overgrow or are aligned parallel to the pre-existing S_1 fabric. Textural relationships and the absence of syn-metamorphic penetrative deformation indicate that M_2 developed under largely static conditions. A subsequent deformation phase (D_2) produced crenulation cleavage (S_2) that overprints S_1 and postdates peak metamorphic conditions.

Peak metamorphic conditions for the garnet-andalusite-biotite schist and associated foliated metapelites, exposed mainly in the Nanga Pinoh and Nanga Semalam areas, were constrained using combined garnet-biotite-andalusite-quartz (GBAQ) geothermobarometry and phase-equilibria (pseudosection) modeling. These methods yield peak conditions of 525-586° C at 2.0-3.8 kbar, consistent with low-pressure, high-temperature Buchan-type metamorphism. Garnet, although likely nucleated during M_1, was chemically re-equilibrated during M_2 and thus participated in the equilibrium mineral assemblage used for *P-T* estimation. The metamorphic evolution of the Pinoh Metamorphic Rocks, therefore, reflects the combined influence of protolith composition, regional tectonism, and Cretaceous granitoid magmatism within the Schwaner Mountains.

Acknowledgements

This work has been supported by The Academic Excellence Scheme-B Research Grant 2024 from Universitas Gadjah Mada (No. 6529/UN1.P1/PT.01.03/2024). Part of the fieldwork and sample acquisition was conducted in collaboration with and supported by The Research Centre for Nuclear Material and Radioactive Waste Technology of The National Research and Innovation Agency (BRIN). The authors gratefully acknowledge the assistance of fieldwork personnel and local guides for their invaluable support during sample collection and logistical activities in The Schwaner Mountains.

References

Adachi, T., Osanai, Y., Nakano, N., and Owada, M., 2012. LA-ICP-MS U-Pb zircon ages and FE-EPMA U-Th-Pb monazite ages of pelitic granulite from the Ukidake area. *Geological Society of Japan*, 118 (1)*,* p.39-52. DOI: 10.5575/geosoc.2011.0022.

Amiruddin and Trail, D.S., 1993. *Geology of the Nangapinoh Sheet area, Kalimantan, Scale 1 : 250,000*, Geological Research and Development Centre, Bandung.

Bemmelen, R.W. van, 1949. The geology of Indonesia, vol. 1A. Government Printing Office, The Hague, 732p.

Bhatia, M.R. and Crook, K.A., 1986. Trace element characteristics of graywackes and tectonic setting discrimination of sedimentary basins. *Contributions to mineralogy and petrology*, 92 (2), p.181-193.DOI: 10.1007/BF00375292.

Bhatia, M.R., 1993. Plate tectonics and geochemical composition of sandstones. *The Journal of Geology*, 91 (6), p.611-627. DOI: 10.1086/628815.

Blandon, G.M., Pieters, P.E., and Supriatna, S., 1989. *Preliminary Report. Catalogue of isotopic ages commissioned by the Indonesia-Australia Geological Mapping Project for igneous and metamorphic rocks in Kalimantan*. Geological Research and Development Centre, Bandung.

Breitfeld, H.T., Davies, L., Hall, R., Armstrong, R., Forster, M., Lister, G., Thirlwall, M., Grassineau, N., Hennig-Breitfeld, J., and Van Hattum, M.W., 2020. Mesozoic Paleo-Pacific subduction beneath SW Borneo: U-Pb geochronology of the Schwaner granitoids and the Pinoh metamorphic group. *Frontiers in Earth Science*, 8, 568715. DOI: 10.3389/feart.2020.568715.

Coggon, R. and Holland, T.J.B., 2002. Mixing properties of phengitic micas and revised garnet-phengite thermobarometers. *Journal of Metamorphic Geology*, 20 (7), p.683-696. DOI: 10.1046/j.1525-1314.2002.00395.x.

Connolly, J.A., 2005. Computation of phase equilibria by linear programming: a tool for geodynamic modeling and its application to subduction zone decarbonization. *Earth and Planetary Science Letters*, 236 (1-2), p.524-541. 10.1016/j.epsl.2005.04.033.

Cox, R., Lowe, D.R., and Cullers, R.L., 1995. The influence of sediment recycling and basement composition on the evolution of mudrock chemistry in the southwestern United States. *Geochimica et Cosmochimica Acta*, 59 (14), p.2919-2940. DOI: 10.1016/0016-7037(95)00185-9.

Davies, L., Hall, R., and Armstrong, R., 2014. Cretaceous crust in SW Borneo: petrological, geochemical and geochronological constraints from the Schwaner Mountains, In *Proceedings Indonesian Petroleum Association, 38th annual convention and exhibition*. IPA14-G-025.

Deer, W.A., Howie, R.A., and Zussman, J., 2013. *An introduction to the rock-forming minerals*. 2^{ed}. Mineralogical Society of Great Britain and Ireland, 696p.

De Kamp, P.C. van and Leake, B.E., 1985. Petrography and geochemistry of feldspathic and mafic sediments of the northeastern Pacific margin. Earth and Environmental Science Transactions of the Royal Society of Edinburgh, 76 (4), p.411-449. DOI: 10.1017/S0263593300010646.

De Keyser, F. and Rustandi, E., 1993. *Geology of the Ketapang sheet area, Scale 1: 250,000*, Kalimantan. Geological Research and Development Centre, Bandung.

Droop, G.T.R., 1987. A general equation for estimating Fe^{3+} concentrations in ferromagnesian silicates and oxides from microprobe analyses, using stoichiometric criteria. *Mineralogical Magazine*, 51 (361), p.431-435. DOI: 10.1180/minmag.1987.051.361.10.

El-Enen, M.M.A., 2011. Geochemistry, provenance, and metamorphic evolution of Gabal Samra Neoproterozoic metapelites, Sinai, Egypt. *Journal of African Earth Sciences*, 59 (2-3), p.269-282. DOI: 10.1016/j.jafrearsci.2010.11.002.

Eskola, P., 1915. On the Relations between the chemical and mineralogical composition in the metamorphic rocks of the Orijärvi Region. *Bulletin de la Commission Géologique de Finland*, 44, p.109-145 (in Swedish with English summary).

Fedo, C.M., Wayne Nesbitt, H., and Young, G.M., 1995. Unraveling the effects of potassium metasomatism in sedimentary rocks and paleosols, with implications for paleoweathering conditions and provenance. *Geology*, 23 (10), p.921-924. DOI: 10.1130/0091-7613(1995)023<0921:UTEOPM>2.-3.CO;2.

Garcia, D., Coelho, J., Perrin, M., 1991. Fractionation between TiO_2 and Zr as a measure of sorting within shale and sandstone series (northern Portugal). *European Journal of Mineralogy,* 3, p.401-414. DOI: 10.1127/ejm/3/2/0401.

Girty, G.H., Ridge, D.L., Knaack, C., Johnson, D., and Al-Riyami, R.K., 1996. Provenance and depositional setting of Paleozoic chert and argillite, Sierra Nevada, California. *Journal of Sedimentary Research*, 66 (1), p.107-118. DOI: 10.1306/D42682CA-2B26-11D7-8648000102C1865D.

Grandstaff, D.E., Edelman, M.J., Foster, R.W., Zbinden, E., and Kimberley, M.M., 1986. Chemistry and mineralogy of Precambrian paleosols at the base of the Dominion and Pongola Groups (Transvaal, South Africa). *Precambrian Research*, 32 (2-3), p.97-131. DOI: 10.1016/0301-9268(86)90003-3.

Gunawan, I., Hall, R., and Sevastjanova, I., 2012. Age, Character and Provenance of the Tipuma Formation, West Papua: New Insights from Detrital Zircon Dating, in *Proceedings Indonesian Petroleum Association, 36th annual convention and exhibition*. IPA12-G-027.

Haile, N.S., 1974. Borneo. In: Spencer, A.M. (ed.), Mesozoic-Cenozoic orogenic belts: data for orogenic studies. *Geological Society, London, Special Publications*, 4 (1), p.333-347.

Hall, R., 2012. Late Jurassic-Cenozoic reconstructions of the Indonesian region and the Indian Ocean. *Tectonophysics,* 570, p.1-41.

Harnois, L., 1988. The CIW index: a new chemical index of weathering. *Sedimentary geology*, 55 (3), p.319-322. DOI: 10.1016/0037-0738(88)90137-6.

Hattum, M.W.A. van, Hall, R., Pickard, A.L., and Nichols, G.J., 2013. Provenance and geochronology of Cenozoic sandstones of northern Borneo. *Journal of Asian Earth Sciences,* 76, p.266-282. DOI: 10.1016/j.jseaes.2013.02.033.

Häussinger, H., Okrusch, M., Scheepers, D., 1993. Geochemistry of premetamorphic hydrothermal alteration of metasedimentary rocks associated with the Gorob massive sulphide prospect, Damara Orogen, Namibia. *Economic Geology,* 88, p.72-90. DOI: 10.2113/gsecongeo.88.1.72.

Hennig, J., Breitfeld, H.T., Hall, R., and Nugraha, A.S., 2017. The Mesozoic tectono-magmatic evolution at the Paleo-Pacific subduction zone in West Borneo. *Gondwana Research*, 48, p.292-310. DOI: 10.1016/j.gr.2017.05.001.

Herron, M.M., 1988. Geochemical classification of terrigenous sands and shales from core or log data. *Journal of Sedimentary Research*, 58 (5), p.820-829. DOI: 10.1306/212F8E77-2B24-11D7-8648000102C1865D.

Holdaway, M.J., 2000. Application of new experimental and garnet Margules data to the garnet-biotite geothermometer. *American Mineralogist*, 85 (7-8), p.881-892. DOI: 10.2138/am-2000-0701.

Holland, T.J.B. and Powell, R.T.J.B., 1998. An internally consistent thermodynamic data set for phases of petrological interest. *Journal of Metamorphic Geology*, 16 (3), p.309-343. DOI: 10.1111/j.1525-1314.1998.00140.x.

McLennan, S.M., Taylor, S.R., McCulloch, M.T., and Maynard, J.B., 1990. Geochemical and Nd-Sr isotopic composition of deep-sea turbidites: crustal evolution and plate tectonic associations. *Geochimica et cosmochimica acta*, 54 (7), p.2015-2050. DOI: 10.1016/0016-7037(90)90269-Q.

McLennan, S.M. and Hemming, S., 1992. Samarium/neodymium elemental and isotopic systematics in sedimentary rocks. *Geochimica et Cosmochimica Acta*, 56 (3), p.887-898. DOI: 10.1016/0016-7037(92)90034-G.

Metcalfe, I., 1988. Origin and assembly of south-east Asian continental terranes. *Geological Society, London, Special Publications*, 37 (1), p.101-118. DOI: 10.1144/GSL.SP.1988.037.01.08.

Nesbitt, H.W. and Markovics, G., 1980. Chemical processes affecting alkalis and alkaline earths during continental weathering. *Geochimica et Cosmochimica Acta*, 44 (11), p.1659-1666. DOI: 10.1016/0016-7037(80)90218-5.

Nesbitt, H. and Young, G.M., 1982. Early Proterozoic climates and plate motions inferred from major element chemistry of lutites. *Nature*, 299 (5885), p.715-717. DOI: 10.1038/299715a0.

Pieters, P.E. and Sanyoto, P., 1993. *Geology of the Pontianak/Nangataman Sheet area, Kaliman-*

tan, Scale 1: 250,000. Geological Research and Development Centre, Bandung.

Qian, X., Yu, Y., Wang, Y., Gan, C., Zhang, Y., and Asis, J.B., 2022. Late Cretaceous nature of SW Borneo and paleo-Pacific subduction: New insights from the granitoids in the Schwaner Mountains. *Lithosphere*, 2022 (1), 8483732. DOI: 10.2113/ 2022/8483732.

Roser, B.P. and Korsch, R.J., 1988. Provenance signatures of sandstone-mudstone suites determined using discriminant function analysis of major-element data. *Chemical geology*, 67 (1-2), p.119-139. DOI: 10.1016/0009-2541(88)90010-1.

Serra-Varela, S., Verdecchia, S.O., Lembo Wuest, C.I., Benítez, M.E., Murra, J.A., and Baldo, E., 2024. Polymetamorphic P-T evolution of the andalusite-garnet-staurolite-sillimanite-bearing schist from the Cushamen Complex (Argentina). *International Journal of Earth Sciences*, 113 (6), p. 1385-1406. https://doi.org/10.1007/s00531-024-02437-3.

Setiawan, N.I., Osanai, Y., Nakano, N., Adachi, T., Setiadji, L.D., and Wahyudiono, J., 2013. Late Triassic metatonalite from the Schwaner Mountains in West Kalimantan and its contribution to sedimentary provenance in the Sundaland. *Berita Sedimentologi*, 28 (1), p.5-13. DOI: 10.51835/bsed.2013.28.1.150.

Tate, R.B., 1991. Cross-border correlation of geological formations in Sarawak and Kalimantan, *Bulletin of the Geological Society of Malaysia*, 28, p.63-95. DOI: 10.7186/bgsm28199104.

Taylor, S.R. and McLennan, S.M., 1985. *The continental crust: its composition and evolution*, Blackwell Scientific Publications, Oxford, 312p.

Varga, A. R. and Szakmány, G., 2004. Geochemistry and provenance of the upper carboniferous sandstones from Borehole Diósviszló-3 (Téseny Sandstone Formation, SW Hungary). *Acta Mineralogica-Petrographica, Szeged*, 45 (2), p.7-14.

Wang, Y., Liu, Z., Murtadha, S., Cawood, P.A., Qian, X., Ghani, A., Gan, C., Zhang, Y., Wang, Y., Li, S., and Zhang, P., 2022. Jurassic subduction of the Paleo-Pacific plate in Southeast Asia: New insights from the igneous and sedimentary rocks in West Borneo. *Journal of Asian Earth Sciences*, 232, 105111. DOI: 10.1016 /j.jseaes.2022.105111.

Weaver, C.E., 1989. *Clays, Muds and Shales*. *Developments in Sedimentology*, *44*, 818 pp.

White, R.W., Pomroy, N.E., and Powell, R., 2005. An in situ metatexite-diatexite transition in upper amphibolite facies rocks from Broken Hill, Australia. *Journal of Metamorphic Geology*, p.579-602. DOI: 10.1111/j.1525-1314.2005.00597.x.

Whitney, D.L. and Evans, B.W., 2010. Abbreviations for names of rock-forming minerals. *American Mineralogist*, 95 (1), p.185-187. DOI: 10.2138/am. 2010.3371.

Williams, P.R., Johnston, C.R., Almond, R.A., and Simamora, W.H., 1988. Late Cretaceous to early Tertiary structural elements of West Kalimantan. *Tectonophysics*, 148 (3-4), p.279-297. DOI: 10.1016/0040-1951(88)90135-7.

Winkler, 1979. *Petrogenesis of Metamorphic Rocks*, 5th ed. Springer, Berlin, 348p.

Witts, D., Hall, R., Nichols, G., and Morley, R., 2012. A new depositional and provenance model for the Tanjung Formation, Barito Basin, SE Kalimantan, Indonesia. *Journal of Asian Earth Sciences*, 56, p.77-104. DOI: 10.1016/j.jseaes.2012.04.022.

Wu, C.M., 2017. Calibration of the garnet-biotite-Al_2SiO_5-quartz geobarometer for metapelites. *Journal of Metamorphic Geology*, 35 (9), p.983-998. DOI: 10.1111/jmg.12264.